

**GRAPHENE TEXTILES TOWARDS SOFT WEARABLE  
INTERFACES FOR ELECTROOCULAR REMOTE CONTROL OF  
OBJECTS**

by  
ATA JEDARI GOLPARVAR

Submitted to the Graduate School of Engineering and Natural Sciences  
in partial fulfilment of  
the requirements for the degree of Master of Science

Sabancı University  
July 2019

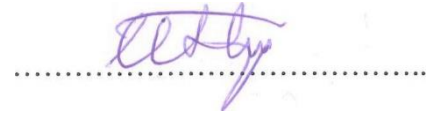
**GRAPHENE TEXTILES TOWARDS SOFT WEARABLE  
INTERFACES FOR ELECTROOCULAR REMOTE CONTROL OF  
OBJECTS**

Approved by:

Asst. Prof. Dr. Murat Kaya Yapıcı  
(Thesis Supervisor)



Assoc. Prof. Dr. Ilker Hamzaoglu



Prof. Dr. Fatih Uğurdağ



Approval Date: July 19, 2019

ATA JEDARI GOLPARVAR 2019 ©

All Rights Reserved

## ABSTRACT

# GRAPHENE TEXTILES TOWARDS SOFT WEARABLE INTERFACES FOR ELECTROOCULAR REMOTE CONTROL OF OBJECTS

ATA JEDARI GOLPARVAR

ELECTRONICS ENGINEERING M.Sc. THESIS, July 2019

Thesis Supervisor: Asst. Prof. Dr. Murat Kaya Yapici

Keywords: EOG, e-textile, graphene, HCI, wearable electronics, eye tracking

Study of eye movements (EMs) and measurement of the resulting biopotentials, referred to as electrooculography (EOG), may find increasing use in applications within the domain of activity recognition, context awareness, mobile human-computer interaction (HCI) applications, and personalized medicine provided that the limitations of conventional “wet” electrodes are addressed. To overcome the limitations of conventional electrodes, this work, reports for the first time the use and characterization of graphene-based electroconductive textile electrodes for EOG acquisition using a custom-designed embedded eye tracker. This self-contained wearable device consists of a headband with integrated textile electrodes and a small, pocket-worn, battery-powered hardware with real-time signal processing which can stream data to a remote device over Bluetooth. The feasibility of the developed gel-free, flexible, dry textile electrodes was experimentally authenticated through side-by-side comparison with pre-gelled, wet, silver/silver chloride (Ag/AgCl) electrodes, where the simultaneously and asynchronous recorded signals displayed correlation of up to ~87% and ~91% respectively over durations reaching hundred seconds and repeated on several participants. Additionally, an automatic EM detection algorithm is developed and the performance of the graphene-embedded “all-textile” EM sensor and its application as a control element toward HCI is experimentally demonstrated. The excellent success rate ranging from 85% up to 100% for eleven different EM patterns demonstrates the applicability of the proposed algorithm in wearable EOG-based sensing and HCI applications with graphene textiles. The system-level integration and the holistic design approach presented herein which starts from fundamental materials level up to the architecture and algorithm stage is highlighted and will be instrumental to advance the state-of-the-art in wearable electronic devices based on sensing and processing of electrooculograms.

## ÖZET

# ELEKTROOKULAR NESNE KONTROLUNDE GRAFEN TEKSTİL ARAYUZ KULLANIMI

ATA JEDARI GOLPARVAR

ELEKTRONİK MÜHENDİSLİĞİ YÜKSEK LİSANS TEZİ, TEMMUZ 2019

Tez Danışmanı: Dr. Öğr. Üyesi Murat Kaya Yapıcı

Anahtar Kelimeler: EOG, e-tekstil, grafen, HCI, giyilebilir elektronikler, göz takibi

Göz hareketlerinin incelenmesi ve bu hareketlerle beraber ortaya çıkan biopotansiyellerin ölçümü, klinik ıslak elektrotların kısıtlamalarının çözülmesi halinde mobil insan bilgisayar etkileşiminde (HCI) ve kişiye özel tıp uygulamalarında artan bir kullanım bulabilir. Bu çalışma klinik elektrotların elektro okülografideki (EOG) kısıtlamalarını çözmek üzere, grafen bazlı iletken tekstillerin ilk defa kullanılmasını ve özelliklerinin belirlenmesini içermektedir ve bu işlem özel tasarlanmış bir gömülü göz izleyici donanımını kullanılmıştır. Bu kendi kendine yeten giyilebilir cihaz, entegre tekstil elektrotlara sahip bir kafa bandından ve Bluetooth üzerinden uzak bir cihaza veri aktarabilen gerçek zamanlı sinyal işlemeli küçük pille çalışan bir donanımdan oluşmakta. Jelsiz, esnek ve kuru grafen elektrotun uygunluğu deneysel olarak ıslak gümüş/gümüş klorür (Ag/AgCl) elektrotlar ile karşılaştırılarak gösterilmiştir. Farklı katılımcılarla yüz saniye boyunca eş zamanlı ve asenkron olarak tekrar edilen ölçümler sırasıyla %87 ve %91'e varan korelasyonlara ulaştı. Ek olarak otomatik göz hareketi tespit algoritması geliştirildi ve böylece grafenli göz hareketi sensörünün HCI kontrol elemanı olarak kullanılabilirliği deneysel olarak gösterildi. On bir farklı göz hareketi biçiminin %85 ve %100 arasında değişen başarılı tespit oranı, önerilen algoritmanın grafen bazlı EOG ölçüm ve HCI uygulamalarındaki kullanılabilirliğini gösterdi. Burada öne çıkarılan sistem seviyesinde ve bütünsel dizayn yaklaşımları gelişmiş EOG sistemlerinin ilerlemesinde faydalı olması beklenmektedir.

## ACKNOWLEDGEMENTS

I would like, hereby, to extend my deepest gratitude to Professor Murat Kaya Yapici, my advisor, for his patient guidance, enthusiastic encouragement, and useful critiques. He consistently allowed my research articles to be my own work but steered me in the right direction whenever he thought I needed it. Without his assistance and dedicated involvement in every step throughout the process, this work would have never been accomplished. I was very lucky to join your lab early on and I have learned so much from you as you created a group of great people and an environment that leaves nothing to be desired as we all pursued exciting research directions.

Nobody wrote a thesis alone, and nobody ever wrote one without the morale-boosting distractions created by friends, and I have many, many people to thank for listening to and, at times, having to tolerate me. I cannot begin to express my gratitude and appreciation for their friendship who are accepting nothing less than excellent from me. My roommate and lab mate Ozberk Ozturk for the stimulating discussions. With his own brand of humour, Abdul Rahman Dabbour has been supportive to me over the years. Thanks are owed to my colleagues Rayan Bajwa, Gizem Acar, Osman Sahin, Farid Sayar Irani, and Melih Can Tasdelen who have been unwavering in their personal and professional support as well as everyone in the *Acoustics Group* at Sabanci University, it was great sharing laboratory with all of you.

I place on record, my sincere appreciation to Mitra Ebrahimpoor, for continuous motivation, to be my mentor through all the way into the grad school. Thank you cousin!

Finally, I must express my very profound gratitude to my parents, who offered their encouragement through phone calls— despite my own limited devotion to correspondence. This accomplishment stands as a testament to your unconditional love, Çox Sağolun.

*In loving memory of my grandmother Lətif*

## TABLE OF CONTENTS

|  |    |
|--|----|
| CHAPTER I.....   | 1  |
| INTRODUCTION AND MOTIVATION .....  | 1  |
| 1.1. Motivation .....  | 1  |
| 1.2. Summary of Works .....  | 1  |
| 1.3. Outline.....  | 2  |
| CHAPTER II.....  | 4  |
| BACKGROUND ON ELECTROOCULOGRAPHY .....   | 4  |
| 2.1. Eye Tracking .....  | 4  |
| 2.2. Limitations of Biopotential Sensing based Oculography.....  | 7  |
| 2.3. Electroconductive Textile Electrodes .....  | 10 |
| 2.4. Dip-coating.....  | 12 |
| 2.5. Related work .....  | 13 |
| CHAPTER III .....  | 15 |
| DEVELOPMENT OF WEARABLE GRAPHENE TEXTILE-BASED EOG<br>PROTOTYPE FROM MATERIALS UP TO SYSTEM-LEVEL..... | 15 |
| 3.1. Synthesis and Integration of Graphene Textile Electrodes .....                                    | 15 |
| 3.2. System-level Architecture .....   | 20 |
| 3.3. Experimental Performance Characterization .....   | 26 |
| 3.3.1. Simultaneous Experiments from Single Subject .....  | 27 |
| 3.3.2. Simultaneous Experiments from Two Subjects .....  | 31 |
| 3.3.3. Asynchronous Experiments from Single Subject.....   | 32 |
| 3.3.4. Electrode Size Tuning Characterization .....  | 33 |
| CHAPTER IV .....   | 35 |



|   |    |
|---|----|
| REMOTE CONTROL OF OBJECTS FOR HCI/HMI APPLICATIONS .....  | 35 |
| 4.1. Pattern Recognition.....                             | 37 |
| 4.2. Feature Extraction .....                             | 38 |
| 4.3. Classification.....                                  | 38 |
| 4.4. Proof of Concept Experiments .....                   | 41 |
| 4.4.1. Blink Controlled Clock Transaction Experiment..... | 41 |
| 4.4.2. Pattern of “8” Trace Experiment .....              | 42 |
| 4.4.3. Long term Durability Experiment .....              | 42 |
| 4.4.4. Eye Mouse Experiment .....                         | 47 |
| CHAPTER V .....   | 49 |
| CONCLUSIONS .....   | 49 |
| BIBLIOGRAPHY.....   | 52 |
| Appendix A.....   | 64 |
| Appendix B: Supplementary Information.....                | 65 |

## LIST OF TABLES

|   |    |
|---|----|
| Table I. Component values and specifications for the front-end circuitry .....  | 22 |
| Table II. Correlation coefficients between signals acquired with graphene textile and Ag/AgCl electrodes.....                     | 30 |
| Table III. Tabular summary of success rate of the automatic detection of eye moves in different scenarios in 1-hour long EOG..... | 46 |

## LIST OF FIGURES

|  |    |
|--|----|
| Figure 2.1. Current technologies for tracking EMs which are either invasive, expensive, or bulky and are not meeting the non-clinical application needs .....  | 5  |
| Figure 2.2. General view of an EOG measurement system where the electrode which cornea is approaching to incurs more positive charges than the other one and results to a unique voltage fluctuation which depends directly on the angle of the eye .....  | 6  |
| Figure 2.3. Reaction of skin to adhesive Ag/AgCl after 6 hours of EOG recording.....   | 9  |
| Figure 2.4. (a) A capacitive coupling based dry electrode made from standard PCB; (b) a penetrative-based needle-shaped electrode and the close-up is a scanning electron microscope photograph; (C) Ag/AgCl coated polyurethane surface electrode in centimetre size .....  | 9  |
| Figure 2.5. The six primary methods of realizing conductive textiles .....   | 11 |
| Figure 2.6. Wearable elastic garments; (a) headband developed for gesture recognition; (b) headband used for horizontal EOG acquisition; (c) eye mask developed for sleep monitoring.....  | 14 |
| Figure 3.1. Block diagram of the proposed EOG-based eye tracker interface .....  | 15 |
| Figure 3.2. Schematic summary of the “dip-dry-reduce” method for the synthesis of graphene textiles along with an image of the prepared graphene-coated e-textile where the inset shows the electrode assembly for prototyping .....   | 16 |
| Figure 3.3. EOG headband with graphene textile electrodes for HCI/HMI applications; insets show flexible graphene textiles after synthesis (bottom right) and stand-alone version of a pair of graphene textile electrodes with foam padding and snap fasteners prior to headband integration (top left).....  | 16 |
| Figure 3.4. Typical electrode placements for hEOG and vEOG .....   | 17 |
| Figure 3.5. Systematic analysis of electrode positioning in forehead EOG. The fabricated electrodes were cut into $\sim 3 \times 3$ cm dimension to test different placement configurations. Waveforms show the induced electrooculograms from (a) locations 4, 6, 8; (b) locations 5, 6, 7; (c) locations 1, 2, 3; (d) locations 5, 6, 8; (e) locations 4, 6, 7; where the first, |    |

second, and third digit corresponds to the location of the left, reference, and the right lead, respectively. The performed eye movements were: (I) voluntary blink, (II) slow left, (III) slow right, (IV) swift left, and (V) swift right ..... 18

Figure 3.6. Fabric active electrode; zoomed-in shows a front-side of the electrode where the graphene-based textile electrode is and the size of the designed buffer circuitry with its component values..... 20

Figure 3.7. The hardware-level schematic of the analog section of the signal conditioning unit (frequency bandwidth: 0.3–10 Hz, adjustable gain: 600–4600 V/V) for the successful acquisition of the EMs, along with experimentally measured signals at the output of each block..... 22

Figure 3.8 EOG signal after smoothing in the  $\mu$ CU which is displayed in real-time through the preliminary Microsoft Excel-based GUI ..... 24

Figure 3.9. 4 generations of designed hardware's for EOG acquisition starting from breadboard prototype, to single-sided PCB, to SMD components assembled PCB, and the final smaller version where microcontroller is also mounted on the system..... 25

Figure 3.10. The hardware level schematic of the portable, battery-powered, EOG acquisition unit including onboard filtering and gain stages in front-end circuitry, power management section, microcontroller unit to process and send information wirelessly to a computer, and a custom-design GUI in LabVIEW. .... 26

Figure 3.11. Schematic diagram showing the position of the eyeballs with respect to specific gaze points located straight ahead in the center (X0), towards the left (X1) and right (X2), along with a tabular summary of the sequence of EMs in the three-stage testing protocol. .... 28

Figure 3.12. (a) Subset of EOG recordings obtained using graphene textile and Ag/AgCl electrodes that displayed the highest correlation among the 2 trials on 8 different participants; (b) zoom-in EOG signals showing the unique EM patterns acquired from participant 1 using graphene textile electrodes; and (c) Ag/AgCl electrode ..... 30

Figure 3.13. (a) Experimental setup showing the simultaneous acquisition of electrooculograms from two subjects where one is attached with graphene textile electrodes and the other with Ag/AgCl electrodes; (b) plot of the recorded signals. .... 31

Figure 3.14. EOG signal acquired from (a) the developed smart headband showing the unique EM patterns, and (b) Ag/AgCl electrode ..... 32

Figure 3.15. Plot of EOG signals acquired from three different sizes of graphene textile electrodes; inset shows an image of the fabricated electrode samples ..... 33

|   |    |
|---|----|
| Figure 4.1. Summarized flowchart of the developed algorithm for automatic detection of blink along with four different saccadic EMs in single-channel forehead EOG .....  | 36 |
| Figure 4.2. (a) EOG trace showing the different types of auto-detected EMs by the proposed algorithm, zoom-in images of the five exclusive signal patterns corresponding to: (b) voluntary blink; (c) swift left-right saccadic gaze; (d) swift right-left saccadic gaze; (e) left gaze; and (f) right gaze. The labels “UM” (up margin), “BUM” (baseline up margin), “BDM” (baseline down margin), and “DM” (down margin) represent the critical threshold levels. The notations (I) to (IV) stand for amplitudes of blink, swift left-right, left and right movements, respectively; and the labels (1) to (8) correspond to data points between which the duration is measured ..... | 39 |
| Figure 4.3. EOG signals acquired with the smart garment (blue trace), where the recorded signal includes several voluntary blink patterns which can be translated into a series of digital pulses (red trace) to effectively implement blink-controlled clock transitions in real-time for enabling switching requirements of HCI devices. Detection of the spontaneous blinks that occurred in the 22nd, 33rd, and 69th seconds were successfully avoided.....   | 41 |
| Figure 4.4. Plot of the induced EOG signal with inserted interpretations for each movement and their issued direction changes, which are used to control an array of LED by turning them on sequentially to trace a pattern of “8” .....  | 43 |
| Figure 4.5. (a) Zoom-in samples from each performed activity (b) 1 hour-long electrooculogram (c) virtual unit pulses generated by the algorithm displaying different amplitudes according to the detected EMs. 0.1 V and 0.2 V pulses are for slow and swift right EMs, respectively; whereas, pulses with the same amplitude but with negative sign are indicators of slow and swift left EMs. Pulses with highest amplitude correspond to the detection of voluntary blinks .....  | 45 |
| Figure 4.6. Plot of the induced EOG signal with inserted interpretations for each movement, which are used to mimic movements of a mouse cursor to write “SUMEMS” into Microsoft Word Office with the aid of a standard virtual keyboard .....  | 48 |
| Figure S1. Timer Interrupt Serves Routine working block diagram for proposed embedded software .....  | 65 |
| Figure S2. The detailed feature extraction section of the flowchart for the proposed automatic EM detection algorithm .....   | 65 |
| Figure S3. The first part of the detailed classification section of the flowchart for the proposed automatic EM detection algorithm. (S: Swift) .....   | 66 |

Figure S4. The second part of the detailed classification section of the flowchart for the proposed automatic EM detection algorithm..... 67

## LIST OF ABBREVIATIONS

|   |    |
|---|----|
| HCI: Human–Computer Interaction .....     | 1  |
| EOG: Electrooculography.....              | 2  |
| Ag/AgCl: silver/silver chloride.....      | 2  |
| EM: Eye Movement.....                     | 2  |
| HMI: Human–Machine Interfaces .....       | 4  |
| IoT: Internet of Things.....              | 10 |
| CNT: Carbon Nanotube .....                | 12 |
| GO: Graphene Oxide .....                  | 12 |
| MWNT: Multi-Walled Carbon Nanotube.....   | 13 |
| SWNT: Single-Walled Carbon Nanotube.....  | 13 |
| rGO: Reduced Graphene Oxide .....         | 15 |
| hEOG: Horizontal Electrooculography ..... | 17 |
| vEOG: Vertical Electrooculography.....    | 17 |
| ECG: Electrocardiography.....             | 20 |
| EEG: Electroencephalography.....          | 21 |
| EMG: Electromyography.....                | 21 |
| DSP: Digital Signal Processing .....      | 21 |
| GUI: Graphical User Interface.....        | 21 |
| INA: Instrumentation Amplifier .....      | 21 |
| CMRR: Common-Mode Rejection Ratio .....   | 22 |
| LPF: Low-Pass Filter .....                | 22 |
| HPF: High-Pass Filter .....               | 23 |
| ADC: Analog-to-Digital Converter .....    | 23 |
| DRL: Driven-Right Leg.....                | 23 |
| PCB: Printed Circuit Board .....          | 23 |
| SMD: Surface Mount Component .....        | 23 |
| μCU: Microcontroller Unit .....           | 24 |

|                                |    |
|--------------------------------|----|
| UM: Up Margin .....            | 37 |
| BUM: Baseline Up-Margin .....  | 37 |
| BDM: Baseline Down-Margin..... | 37 |
| DM: Down Margin .....          | 37 |
| SR: Success Rate .....         | 42 |



## CHAPTER I

### INTRODUCTION AND MOTIVATION

#### 1.1. Motivation

Eye tracking matters to many. For a brand leader, the prospect of seeing the world through their customers' eyes, literally, as opposed to relying on traditional market research methods is the reason that makes eye tracking a clear step towards objectively understanding what really drives the shopping experience and purchase decisions, at a subconscious level. In virtual reality not only eye tracking does enable a whole new method to interact intuitive with contents, but it could also add another layer of connection and feedback, as well as adding a new means of privacy and security check through retinal scanning. In healthcare, eye tracking enables devices that could help to better ease the challenging life of a disabled individual using their eye motions.

Current technology for eye tracking, however, is lacking to correspond to the necessities of an everyday usable product by every-layers of the society and failed to take challenges of the current era's electronic appliances requirement: to be minimized (both in power consumption and size), wearable, and aesthetic. Therefore, this work aims to suggest an alternative eye tracking system by presenting the first graphene textile-based wearable eye tracker device.

#### 1.2. Summary of Works

The presented work extends the pioneering efforts on wearable graphene textiles toward

object control and mobile Human–Computer Interaction (HCI) and reports, for the first time, successful acquisition of electrooculography (EOG) signals with graphene textile electrodes. It also provides a systematic analysis on the possible locations on the forehead to record ocular biopotentials and describes the system-level integration of textile electrodes into an ordinary elastic sports headband with embedded electronics to realize a highly-integrated, light-weighted, wearable eye tracker device to worn on the body and particularly designed for unobtrusive and long-term daily use.

The specific contributions of this work are (1) feasibility check of graphene textile electrodes in sensing EOG signals experimentally through several case studies with direct comparison to conventional silver/silver chloride (Ag/AgCl) electrodes; (2) the design of a pocket-worn, battery-powered EOG-based eye tracker which implemented as headband and can stream data to a remote device over Bluetooth; (3) design of an automatic detection algorithm to differentiate between different eye movements (EMs) in real-time; (4) the characterization of wearable eye tracker through several experiments as a proof-of-concept demonstration.

### **1.3. Outline**

Parts of this thesis were originally published in “*IEEE Sensors 2017 proceedings*” as *Wearable Graphene Textile-Enabled EOG Sensing* in [1], in “*Body Sensor Networks 2018 proceedings*”, as *Graphene-coated Wearable Textiles for EOG-based Human-Computer Interaction* in [2], in “*IEEE Sensors Journal*” as *Electrooculography by Wearable Graphene Textiles* in [3], in “*MDPI Electronics*” as *Wearable and Flexible Textile Electrodes for Biopotential Signal Monitoring: A review* in [4], and, in “*Journal of The Electrochemical Society*” as *Graphene Smart Textile-Based Wearable Eye Movement Sensor for Electro-Ocular Control and Interaction with Objects* in [5], and are reproduced in detail here.

In this chapter, the target of this research was introduced along with the specific contributions of this work. In the next chapter, the main limitations of current EOG-based eye tracking technology along with some essential background information regarding

physiology of EMs and the state-of-the-art in EM research with particular emphasis on sensors and applications presented. Later on, a literature review covering dry electrodes, textile manufacturing technology, and similar previous work presented. In the third chapter, the fabrication of the textile electrodes and their integration into a wearable garment along with the acquisition circuitry and its design criteria discussed and followed by the characterization of the developed textile electrodes. In the fourth chapter, detailed information on signal processing algorithm to automatically detect EMs is given and the proof-of-concept experiments which critically designed to evaluate the performance of the system is covered. The challenges from fundamental material development to high-level integration are emphasized in chapter five to highlight areas that need development and suggest future directions for further improving the fully integrated wearable eye tracker.

## CHAPTER II

### BACKGROUND ON ELECTROOCULOGRAPHY

#### 2.1. Eye Tracking

Eye stores a tremendous source of potential for the rise of new applications in human-computer/machine interfaces (HCI/HMI), and EMs are known to possess a rich source of information including signatures of emotional states, psychiatric disorders or psychological behaviours, perception, desires, and needs which have been of much interest to cognitive neurosciences [6, 7]. Throughout the past century, eye tracker machines highly evolved and now they can be classified under either of the following concepts: scleral search coil-based oculography, infrared reflection-based oculography, video-oculography, and biopotential measurement-based oculography [8, 9]. Economic challenges and long-term performance of the earlier designs, however, obligates successful realization of casual, consumer-driven, and wearable products (figure 2.1). For instance, coil-based eye tracking systems are invasive and are not meeting the non-clinical application needs (figure 2.1a) [10]. On the other hand, although camera-based eye tracking setups fulfil the invasivity issue and display long-term functionality, they are hardly affordable due to their hardware (e.g. camera) and image processing requirements. For instance, SR Research's camera-based eye tracker products cost a minimum of ~28000 EUR (figures 2.1c and 2.1d). Additionally, in video-oculography, the camera has to be positioned at a location suitable to capture the EMs, which limits portability of such systems. Therefore, effort has been placed to fully investigate different methods to take possession of EMs.

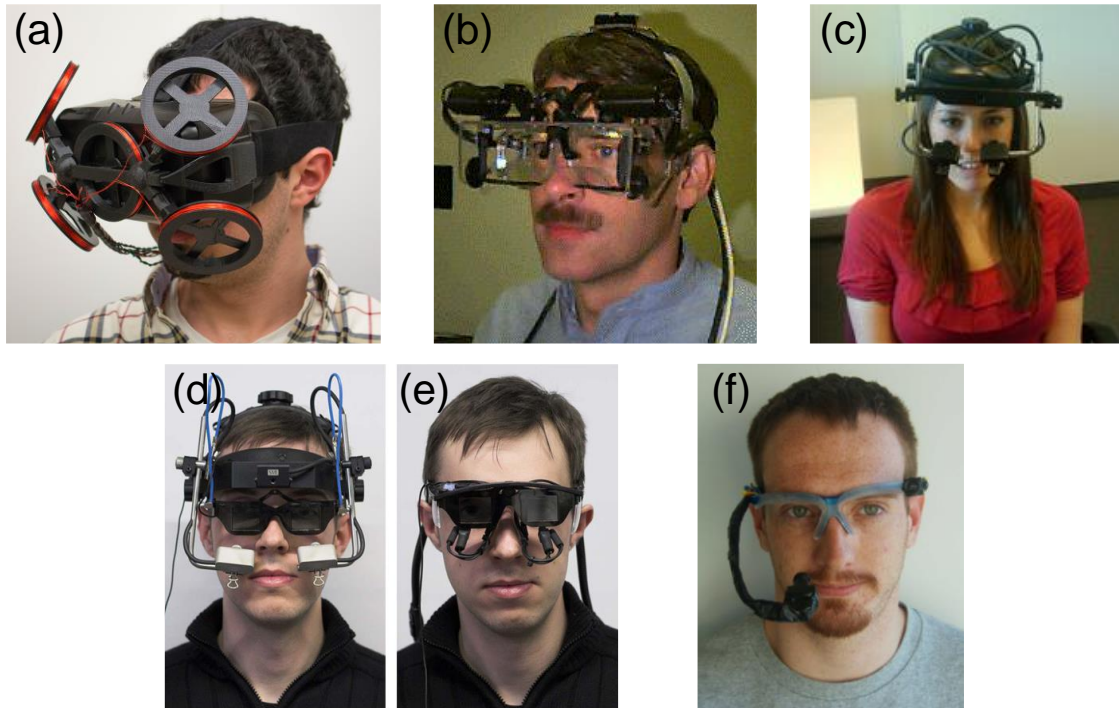


Figure 2.1. Current technologies for tracking EMs which are either invasive, expensive, or bulky and are not meeting the non-clinical application needs. (a) state-of-art search coil-based eye tracking system called EyeContact [11]. (b) Infrared reflection-based eye tracker which equipped with two cameras to track two pupils and reflections of infrared light out of the cornea <sup>1</sup>. Head-mounted video-based eye tracker systems: (c) SR Research EyeLink II used in memory performance investigation [12]; (d) SR Research EyeLink I and (e) Arrington Research ViewPoint PC-60 BS007 which both were used in a Virtual Reality study [13]; (f) the third generation of an open-source and low-cost (comparatively) solution called openEyes [14].

Alternatively, EOG is an economical (a normal EOG set-up could be assembled under 100 EUR [15]), non-invasive, and reliable method for acquiring biopotential signals around the eyes, and addresses the limitations of both coil- and camera-based systems [9] and has estimated precision of up to  $1.5^\circ$  [16]. EOG is essentially based on the simple model of the human eye, which is a dipole with permanent potential difference between its forward and backward facing spots (cornea-retinal potential, 0.4-1.0 mV: the cornea being positive) [17]. This potential difference sets up an electrical field in the tissues surrounding the eye which generates an electric field [18].

<sup>1</sup> <http://schorlab.berkeley.edu/research/equipment>

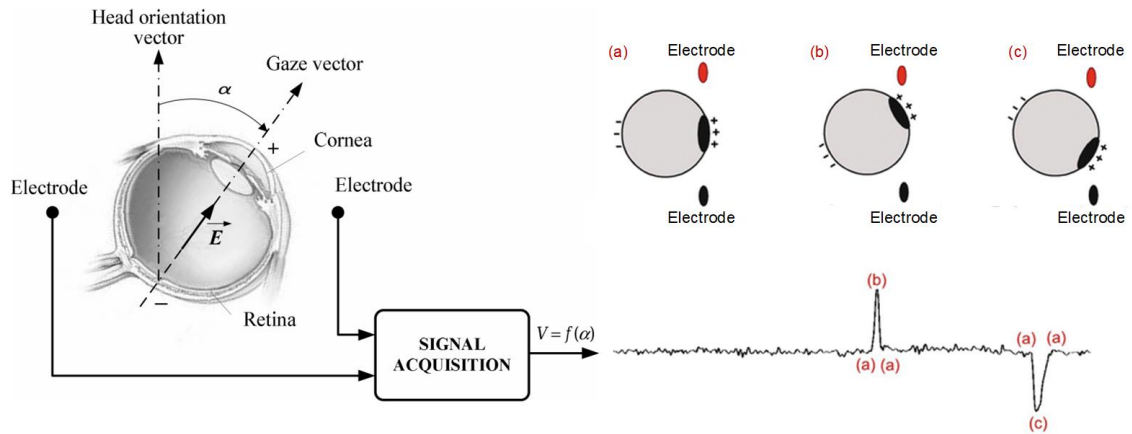


Figure 2.2. General view of an EOG measurement system where the electrode which cornea is approaching to incurs more positive charges than the other one and results to a unique voltage fluctuation which depends directly on the angle of the eye; adapted from [19, 20].

If a pair of electrodes is attached around the eyes, during EMs, the field vector rotates correspondingly and the electrode which cornea is approaching to will incur more positive charges than the other one and the result will be a unique voltage fluctuation which can be detected by the attached electrodes [20]; figure 2.2 illustrates this phenomenon. By analysing these deviations with signal processing techniques, the type of EM can be tracked and determined [21].

The recorded biopotential signals are referred to as the electrooculograms, and the method for acquiring them is termed as EOG [22]. Electrooculograms also occurs in total darkness [23], when the eyes are closed [24], and even in visually impaired people [25]. However, as we will see later on in this work, their signal characteristics may differ. For instance, when the eyes closed, the amplitude of the recorded electrooculograms significantly increases.

Although induced electrooculogram due to wink or blink is comparatively stronger in amplitude to the ones which occur due to lateral or horizontal EMs, the eyes only slightly move (approximately  $5^\circ$ ) in winking or blinking. It's because, in eyelid-related movements, such as closing or opening the eyes, the cornea is short circuits with retina (figuratively speaking) and thus resulting potential is actually the sum of the cornea and retinal potential together [24]. Despite that these eyelid-related boosts are not directly due to EMs, alike prior works, this work considers them as electrooculograms as well.

## **2.2. Limitations of Biopotential Sensing based Oculography**

So far, several EOG-based rehabilitation systems were developed as an assistive technology for people with lock-in syndromes, who have extremely limited peripheral mobility but still retain their eye motor coordination [26], in order to ease their daily life challenges and/or enable them to communicate [27-30]. Similarly, basic deliberate EM such as saccades (i.e. fast EMs), fixations (i.e. duration between to saccades when gaze fixated onto something), and blinks have been used for hands-free operation in HCI/HMI [31-33] and are able to facilitate mouse cursor emulation [34], type in virtual keyboard [35, 36], drive wheelchair [37], control robots [38], change TV channels [39], and even improve user experience on virtual reality gaming [40] or smartphone operation [41]. Additionally, visual fatigue estimation using EOG was proposed to be used in 2D/3D display auto-adjustment switch systems [42].

Along these lines, in the healthcare domain, as part of a hospital alarm system, EOG-based switches provided immobile patients with a safe and reliable way of signaling an alarm [43]. Also, utilization of an EOG-based eye tracking system suggested for controlling of an artificial eye for individuals with the single-eye blind condition to compensate for the movement of their lost eye [44]. Furthermore, EOG found instrumental for diagnosis and treatment of disorders emerging due to excessive or insufficient amount of blinking [45, 46].

Combined with other biopotentials, EOG-included hybrid biopotential monitoring systems are currently being investigated in a vast range of disciplines from emotional states classification and behavioral studies [21] to controlling prosthesis arms [47]. For instance, sleep scoring system based on EOG was reported [48] which later on facilitated to development of a practical eye mask for long-term sleep monitoring experiments [49]. Similarly, real-time drowsiness detection [50] and vigilance estimation were studied using EOG features [51].

Other promising studies were also conducted by EOG-functionalized goggle in monitoring EMs during daily activities [52], such as reading to calculate how fast the reading speed is and the number of covered words [53]. Moreover, recent developments

in EOG research enables the direct entrance of Arabic numbers, English alphabets, and Japanese Katakana by EM which further facilitate users to communicate complicated messages in a relatively short time [54-56]. These all are in turn, strengthen the earlier prediction that the EOG has possibilities of exploiting new kinds of context-aware applications and replace current eye tracking technology [57].

However, despite the various demonstrators of wearable EOG devices in the literature, which proves that EOG is a measurement technique that is reliable, easy to operate, and can be made cosmetically appealing, they struggle to fulfill the needed qualities to become a standard market product and their full potential has not been realized due to limitations of the sensing electrode [57]. Typically, acquisition units for electrophysiological responses (EOG included) rely on the direct contact of disposable, pre-gelled, “wet” Ag/AgCl electrodes fixed on the subject's skin with adhesive backings. Although standard Ag/AgCl electrodes are low-cost, widely available, and provide accurate signal acquisition capabilities [58], while being less crucial for quick short-time measurements, the need for skin preparation severely limits their usability in wearable electronic applications intended for long periods of use like premature infant monitoring [59, 60]. The primary reason for this is due to the discomfort on the user-end caused by the sticky gel layer and adhesive support of the wet electrodes. For instance, the conductive gel dehydrates in time and degrades the electrode performance, thus, once in a few hours, electrodes must be changed or the gel must be re-applied, which is inefficient and time-consuming and not acceptable for everyday and easy to use applications. Moreover, the gel can cause an itching sensation [61]; as well as, red and swollen skin which develops immediately upon removal by mechanical peeling of the electrode. Such irritations and allergic reactions may only last for several hours [1] or may even lead to dermatitis [62]. To demonstrate the severity of the skin irritations three electrodes were attached to the forehead which remained intact during a ~ 6-hour EOG recording session. Even 12 hours after removing electrodes, skin irritation was still observable (figure 2.3).

Due to the above concerns, studies have been proposing the elimination of the gel by developing “dry” electrodes, which are more suitable for continuous, autonomous and unsupervised electrophysiological monitoring, and meet the desired comfort level for integration with wearable devices [63].





Figure 2.3. Reaction of skin to adhesive Ag/AgCl after 6 hours of EOG recording.

Different materials and fabrication techniques have been investigated to realize dry electrodes for biopotential monitoring applications which can be classified into three main categories: capacitive, penetrative, and surface electrodes (figure 2.4) [58]. Capacitively coupled non-contact dry electrodes are isolated from the stratum corneum via an insulating layer (figure 2.4a). This results in high skin-electrode contact impedance, causing the electrodes to be more prone to noise and motion artifacts which place a larger burden on the design of sensitive front-end read-out circuitries [64, 65]. Tip-shaped penetrative contact electrodes circumvent high impedance problems associated with the outermost layer of the skin (i.e. stratum corneum) by piercing into it (figure 2.4b). Such microneedle arrays are fabricated with micromachining techniques and reported to be painless and mechanically stable [61, 66, 67].

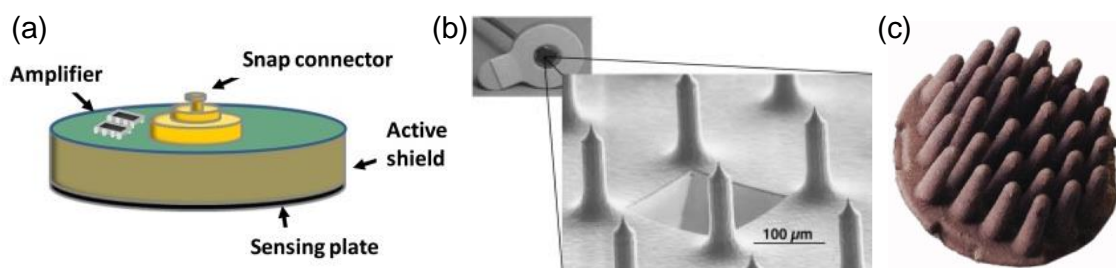


Figure 2.4. (a) A capacitive coupling based dry electrode made from standard PCB [68]. (b) A penetrative-based needle-shaped electrode and the close-up is a scanning electron microscope photograph [66]. (c) Ag/AgCl coated polyurethane surface electrode in centimetre size [69].

Among dry electrodes, surface electrodes are likely to be the most widely used ones, where innovative strategies both from the perspective of electrode geometry and materials have been considered to establish direct contact with the skin surface. For instance, polymeric structures in the form of protruding pin arrays in centimetre scales have been fabricated to allow functioning over hair (figure 2.4c) [70]. Another promising approach that emerged in recent years is based on the use of smart textiles.

### **2.3. Electroconductive Textile Electrodes**

A new trend in electronics nowadays is towards the miniaturization and integration of devices into wearable formats such as smartwatches, garments, and goggles, where the technology is collectively referred to as wearable electronics or wearable computing [71]. The emerging wearable electronics market is expected to grow 15.5% annually from 2016 to 2022. This has created a new venue for researchers to investigate novel approaches and develop robust, compact, reliable, and cost-effective solutions to meet the growing demand for wearable devices. Hence, a thorough investigation of suitable materials, fabrication methodologies, and sensing elements needs to be carried out.

Electronic textile (e-textile) or “smart textile” is an evolving technological platform in the field of wearable electronics that studies the integration of functional materials with ordinary clothing to realize devices including sensors, energy harvesters [72], antennas [73], advanced textiles for self-heating and cooling [74], and even fashion applications [75]. These are achieved by embedding materials with electrical, mechanical, and/or thermal properties into textiles to add desired functionalities for a given application. For instance, materials with unique properties have been used for chemical sensing of sweat [76], temperature [77], and pressure and strain [78]. Moreover, internet of things (IoT)-friendly applications are also possible by the integration of wireless transmission modules into textiles to allow continuous transfer of physiological information to a remote medical unit or to the cloud [79]. The usage of electroconductive textiles promises to add several other advantages including flexibility, permeability to air and moisture, and easy integration to daily clothing [80]. Flexibility is important primarily to enable skin-

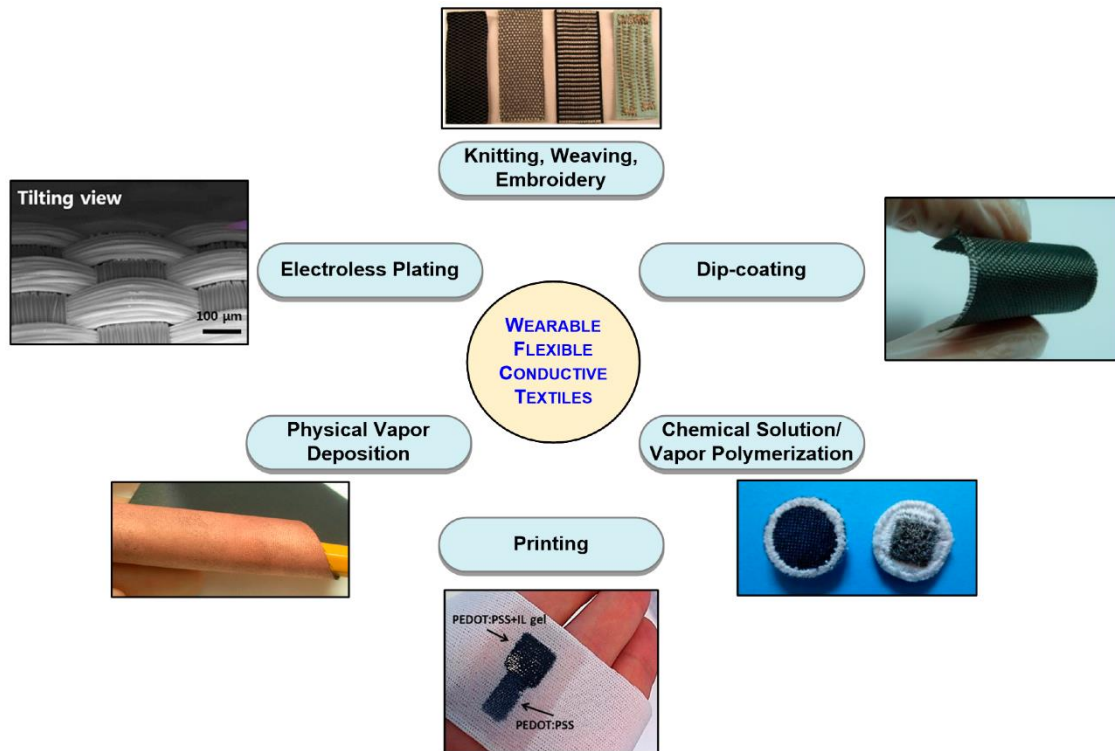


Figure 2.5. The six primary methods of realizing conductive textiles.

compatible devices by matching with the natural contours of the body, to provide wearability, and to achieve better skin-electrode coupling, whereas permeability to air and moisture alleviates the possibility of skin irritations.

Owing to their inherent advantages, several methods have been suggested to develop electroconductive textile electrodes for electrophysiological signal monitoring. The main challenge here is to synthesize conductive textiles from ordinary fabrics and fabrication of e-textiles essentially relies on the stable integration of conductive materials with fabrics and fibers. Commonly used conductive materials include metals, conductive polymers, and carbon allotropes. These materials can be used either with mainstream fabric manufacturing/decoration approaches (e.g. knitting, weaving, embroidery) [81], or can be applied onto finished textiles with various techniques like electroplating [82], physical vapour deposition [83], chemical polymerization [84], and printing methods [85] to coat the surface of the textile (figure 2.5). However, earlier methods either require dedicated equipment or fabrication processes that are complex, expensive, and incompatible for large-scale production, lack uniformity or sacrifice from the natural comfort of the fabric. In order to use textiles as biopotential sensors, they need to be flexible, durable, comfortable, and, biocompatible and have suitable electrical characteristics for signal

acquisition. Several advantages of graphene—a single layer of carbon atoms arranged in a hexagonal lattice, having excellent electrical conductivity and elasticity combined with high ultimate strength while being extremely lightweight [86], leads to the direct application of it in e-textiles. Owing to these features, the merger of graphene on a variety of textiles was recently demonstrated based on a low-cost, gel-free, washable, and scalable approach using dip-coating [87].

## **2.4. Dip-coating**

Dip-coating is one of the simplest methods to coat yarns or fabrics, and it is still used in the textile industry [88]. The simple and scalable nature of dip-coating allows the manufacturing of rolls of conductive fabrics with lower fabrication cost, and after cutting and sewing of the desired patch, it is also possible to attach textile electrodes onto an existing garment [89].

The process consists of the immersion of the substrate in a solution containing conductive materials such as metallic particles [90], conductive polymers [91], or carbon derivatives such as graphene [87] and carbon nanotubes (CNTs) [92]. Upon application of a conductive solution to textiles, excess material is removed [93] and a drying step, known as curing, is performed to evaporate the solvent and fixate the conductive particles on fiber surfaces. To realize a stable coating, surface properties of the textile such as wettability and hydrophilicity are important. Care should also be taken to limit the drying/curing temperatures to avoid potential damage to the textile [94].

Conductive solutions or pastes are the only feasible way to utilize graphene/CNTs in textile coating. Although multiple techniques such as chemical vapor deposition, mechanical exfoliation, epitaxial growth on silicon carbide, and chemical reduction of graphene oxide (GO) exist for preparing graphene [95], the latter approach (i.e., chemical reduction) is the most suitable and applicable for textile surfaces due to low-temperature processing and scalability [96]. In graphene-coated textile preparation, the desired piece of textile is dipped in a GO solution, and subsequent drying provides fixation on fiber surfaces. As for post-processing, a chemical reduction procedure is performed to convert

GO flakes into graphene, allowing electrical conductivity to be imparted [87]. CNT powders have also been used to create conductive fabrics [97]. For instance, textile electrodes were fabricated by cladding cotton fabrics with multi-walled CNTs (MWNT). To ensure their adhesion, a conductive paste made from tapioca starch and MWNT powder was applied to the surface and cured afterward [98]. Another aspect of wearable monitoring was looked into with the creation of conductive cotton yarns to use in biosignal transmission [92]. Regular cotton yarns became conductive with dipping in a single-walled carbon nanotube (SWNT) solution and drying afterward, which fixated SWNTs to cotton microfibrils.

Regarding the biocompatibility of CNTs, while there is some concern regarding their cytotoxicity, the purity of the carbon nanotube (i.e. elimination of trace metals such as iron that get incorporated into CNTs during manufacturing) has been shown to be a critical factor, especially for the case of dermal administration and exposure to CNTs [99]. Arguably, with better control of purity, it may be possible to reduce or eliminate the potential toxicity of CNTs when used as part of conductive textile electrodes placed in direct contact with the skin. Graphene, on the other hand, has been shown to have minimal effects on the skin as long as the concentration and exposure are moderate [100].

## **2.5. Related work**

Using screen and stencil printing processes, an electrode network was fabricated and embedded on a headband and used for horizontal EOG acquisition (figure 2.6a) [101]. Similarly, conductive fabrics used in a headband to measure EOG have been capitalized on in a drowsiness detection application [50]. Additionally, a silver-coated nylon textile was integrated into a headband and adapted for gesture recognition (figure 2.6b) [102]. Silver/polyamide compound textiles have also been employed to develop a wearable eye mask for sleep monitoring and automatic sleep staging (figure 2.6c) [49]. Moreover, novel self-wetting electrodes composed of PEDOT:PSS fibers were integrated into a thin layer of a membrane by dip-coating and then tested in a short (~8 s) EOG experiment where results showed 93% correlation with those of wet electrodes [103]. Furthermore, a novel conductive polymer foam with a conductivity of about 0.07  $\Omega$ /square was

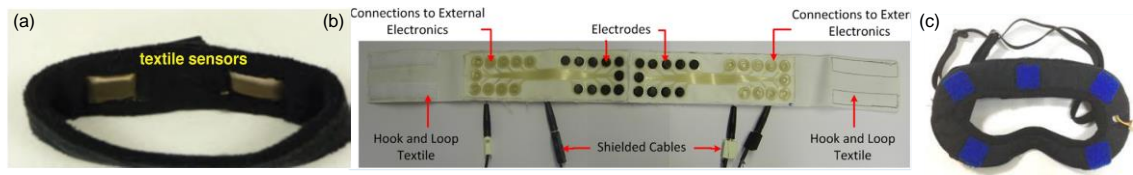


Figure 2.6. Wearable elastic garments; (a) headband developed for gesture recognition [101]; (b) headband used for horizontal EOG acquisition [102]; (c) eye mask developed for sleep monitoring [49].

fabricated and tested in forehead EOG and displayed ~84% correlation against standard electrodes [104].

## CHAPTER III

### DEVELOPMENT OF WEARABLE GRAPHENE TEXTILE-BASED EOG PROTOTYPE FROM MATERIALS UP TO SYSTEM-LEVEL

The block diagram of the proposed eye tracking system consisting of graphene textile embedded smart headband along with front-end read-out circuitry for onboard signal conditioning, microcontroller unit for signal processing, and display for real-time monitoring and visualization is illustrated in figure 3.1. Herein here, this chapter covers the textile preparation and integration of it to a wearable garment, and, the required electronics for acquisition and conditioning of EMs whereas signal processing part will be covered in the next chapter,

#### 3.1. Synthesis and Integration of Graphene Textile Electrodes

Conductive textiles were synthesized based on a low-cost and scalable, three-step dip-

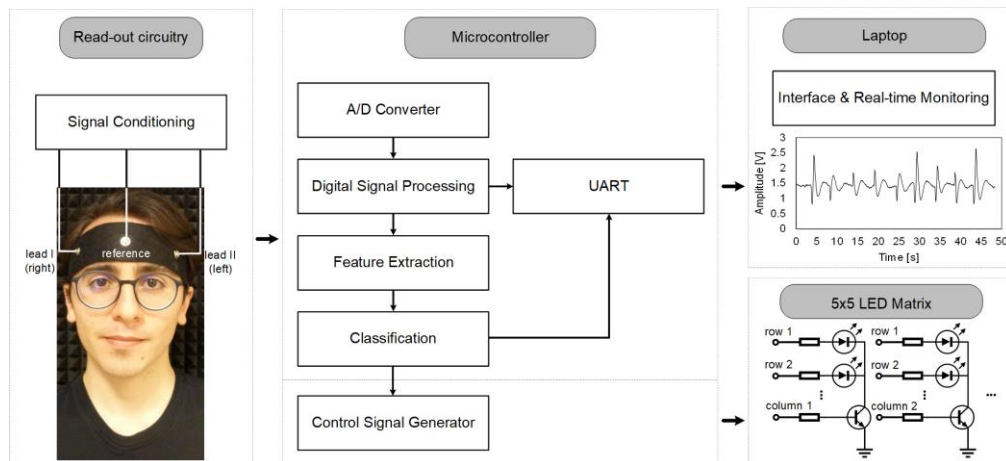


Figure 3.1. Block diagram of the proposed EOG-based eye tracker interface.

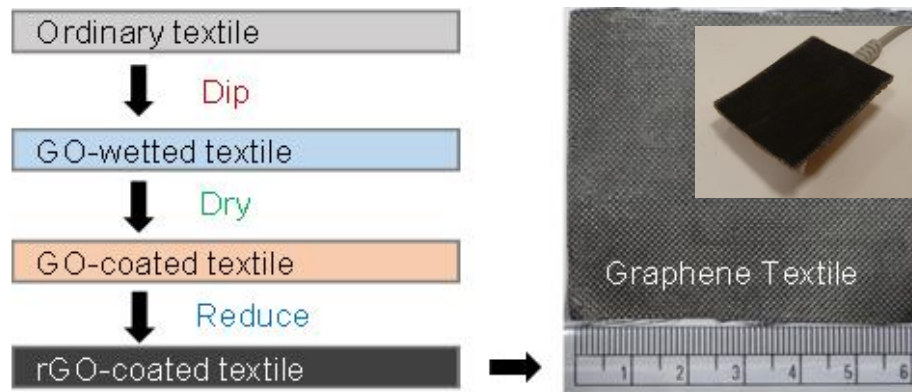


Figure 3.2. Schematic summary of the “dip-dry-reduce” method for the synthesis of graphene textiles along with an image of the prepared graphene-coated e-textile where the inset shows the electrode assembly for prototyping.

coating approach (figure 3.2) where graphene clads around a variety of ordinary fabrics (e.g. nylon, cotton, polyester) forms a conformal layer [87]. The process involved preparation of GO suspension based on the modified Hummer’s method, followed by dipping of plain textiles into GO solution. Next, the wetted textile was left to dry at moderate temperatures ( $\sim 80^{\circ}\text{C}$ ) which allowed layering of GO around individual textile fibers. The GO-coated textile was then chemically treated with reducing agents like hydrazine or hydrogen iodide and rinsed in deionized water to form stable, conductive, reduced graphene oxide (rGO) cladding on textiles. The sheet resistance of the prepared textiles was measured as  $\sim 20 \text{ k}/\text{sq}$  which was determined to be suitable for the required signal levels in the front-end sensor interface circuit. For different applications, it is possible to tune the conductivity by introducing various process modifications [105].

In order to detect electrooculograms from different spots on the forehead, the prepared graphene textile piece was cut into desired dimensions ( $\sim 3 \times 3 \text{ cm}$ ) and mounted on an elastic headband with flexible sticky foams which were sandwiched between metallic snap fasteners in order to establish electrical connection with the front-end circuitry (figure 3.3). To acquire ocular biopotentials, electrodes should be positioned on the skin surface and have stable contact. In commercial electrodes, this is achieved by gels and adhesives; which, on the other hand, limit their use in wearable applications.



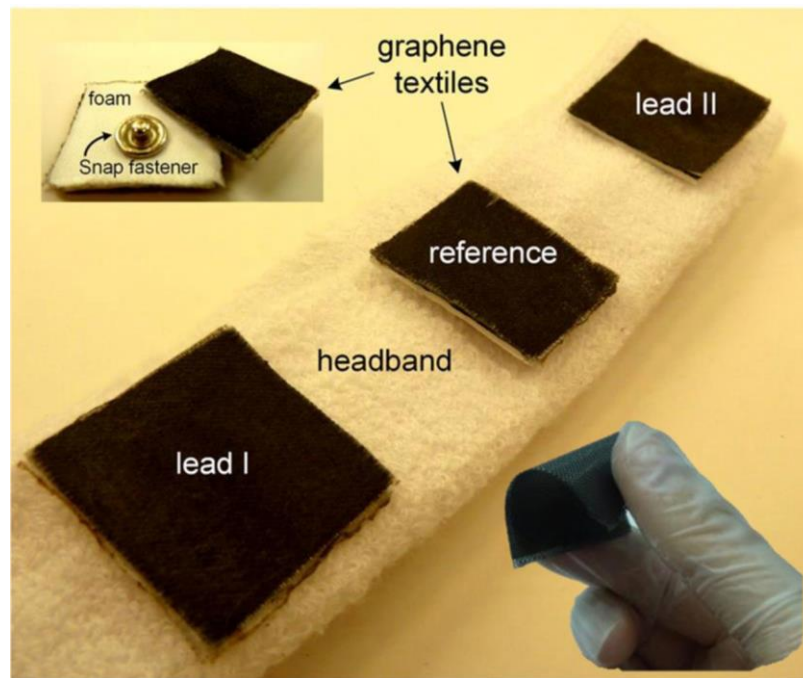


Figure 3.3. EOG headband with graphene textile electrodes for HCI/HMI applications; insets show flexible graphene textiles after synthesis (bottom right) and the stand-alone version of a pair of graphene textile electrodes with foam padding and snap fasteners prior to headband integration (top left).

Alternatively, we have used elastic bands with Velcro straps and foam paddings (polyethylene-based) to provide pressures in the range of few mmHg (up to 5 mmHg) [106], which supported the contact of graphene textile electrodes on the skin surface and ensured interface stability, and at the same time lowers the contact impedance by reducing the air gap between the electrodes and the skin [107].

As we will see later on, the amplitude of the EOG signal is sensitive to relatively small variations in electrode positioning [18], depending on the application, different electrode

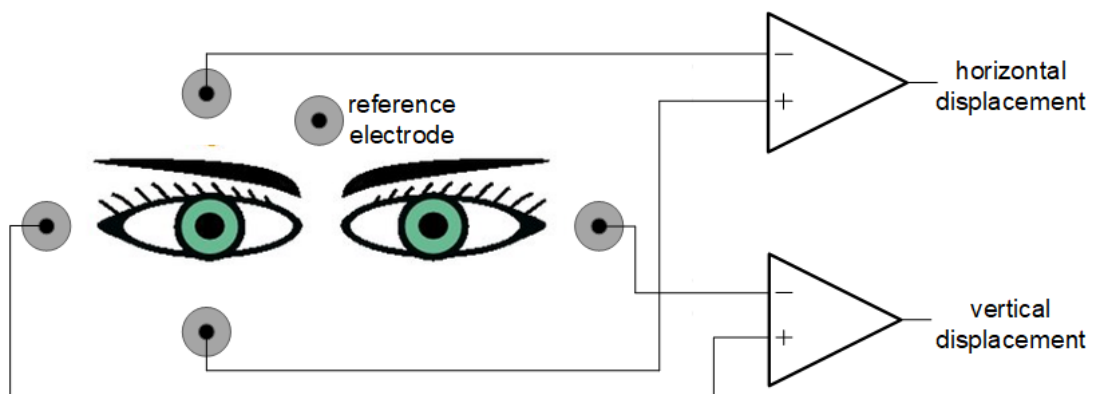


Figure 3.4. Typical electrode placements for hEOG and vEOG.

counts and locations were investigated [19, 25]. Commonly in clinical monitoring, a signal acquisition unit with two channels, one for horizontal EOG (hEOG) and the other for vertical EOG (vEOG), is used to record raw biopotential signal (figure 3.4) [108]. In this configuration, five electrodes are used, where one electrode is placed at the outer canthus of the left and right eye for detecting lateral EMs; whereas the remaining two are attached above and below an eye for picking up transverse eye activity and the last electrode is either placed centrally on the forehead or on the mastoid as a reference [109].

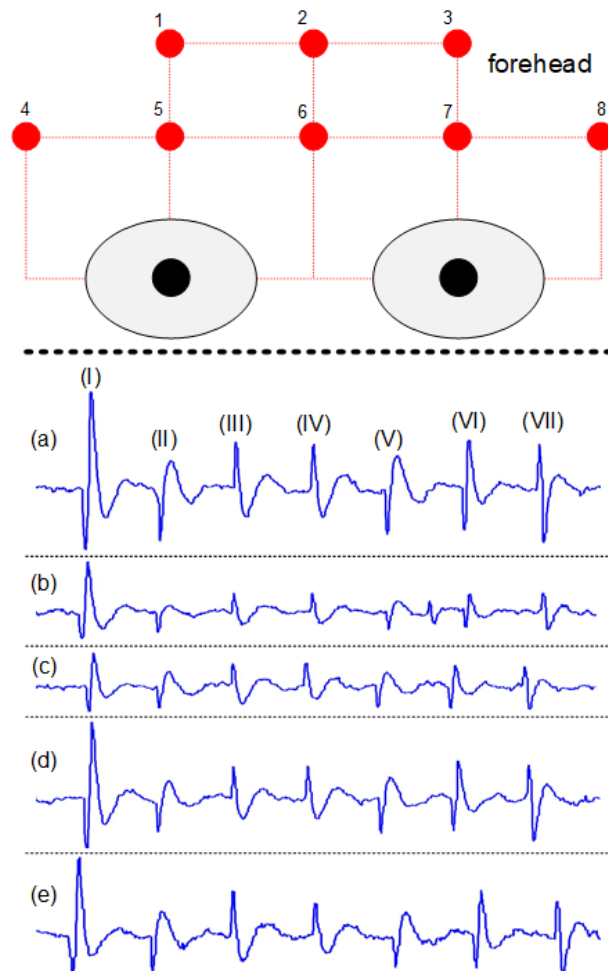


Figure 3.5. Systematic analysis of electrode positioning in forehead EOG. The fabricated electrodes were cut into  $\sim 3 \times 3$  cm dimension to test different placement configurations. Waveforms show the induced electrooculograms from (a) locations 4, 6, 8; (b) locations 5, 6, 7; (c) locations 1, 2, 3; (d) locations 5, 6, 8; (e) locations 4, 6, 7; where the first, second, and third digit corresponds to the location of the left, reference, and the right lead, respectively. The performed EMs were: (I) voluntary blink, (II) slow left, (III) slow right, (IV) swift left, and (V) swift right.

Although in literature, it was suggested that a natural choice for EOG-based wearable garment are goggles and claimed that they minimize distraction to the user [57], alternatively, mask [36, 49], headband [50, 110], and headphones [111] was proposed as host garments as well. Probably considering overall comfort and operability by everybody (i.e., including bespectacled individuals) the most comfortable approach on the user-end for wearable devices to record electrooculograms is only from locations on the forehead and “forehead EOG” is preferred easily by integrating electrodes into elastic headbands.

Mostly, forehead EOG uses two-channel configuration by having four electrodes where one of the electrodes is shared between channels and detects 4 different saccadic movement patterns (i.e. left, right, up, and down EMs) to execute various control commands [110, 112]. Here, we propose a new electrode positioning configuration to detect the same number of differing EM patterns, hence control commands, with only three electrodes and one channel. In this electrode placement, three electrodes are to be fixed on the forehead where two of the electrodes were placed roughly above the left and right eye toward the temples (figure 3.5, locations 4 and 8), and a reference electrode was placed halfway in between (figure 3.5, location 6). This configuration is chosen through an experiment where a volunteer was asked to perform different blink, saccadic and fixation EMs; induced waveforms are included in figure 3.5. First configuration (I) is selected to be the most appropriate one to be automatically identified with thresholding algorithms since amplitudes and patterns of EMs differ a lot in comparison with other configurations and they are stronger in terms of magnitude. A direct benefited of inducing the sufficient amount of comments from a single channel and only three electrodes is the elimination of crosstalk noise between vertical and horizontal channels.

Similar to dry electrodes, textile electrodes generate a high impedance which makes the signal susceptible to physical movements and power line interference. One method to minimize this effect is by reducing the signal-source impedance by utilizing a buffer amplifier which essentially converts the high-impedance signal to a low-impedance one [113]. Figure. 3.6 illustrates the components for building an “active” electrodes which are only an op-amp (OPA2365, Texas Instruments, USA) having high input impedance, two resistors, and one capacitor. Regardless of the merit of active electrodes, there has been some reluctance to use them since they require a power supply [114].

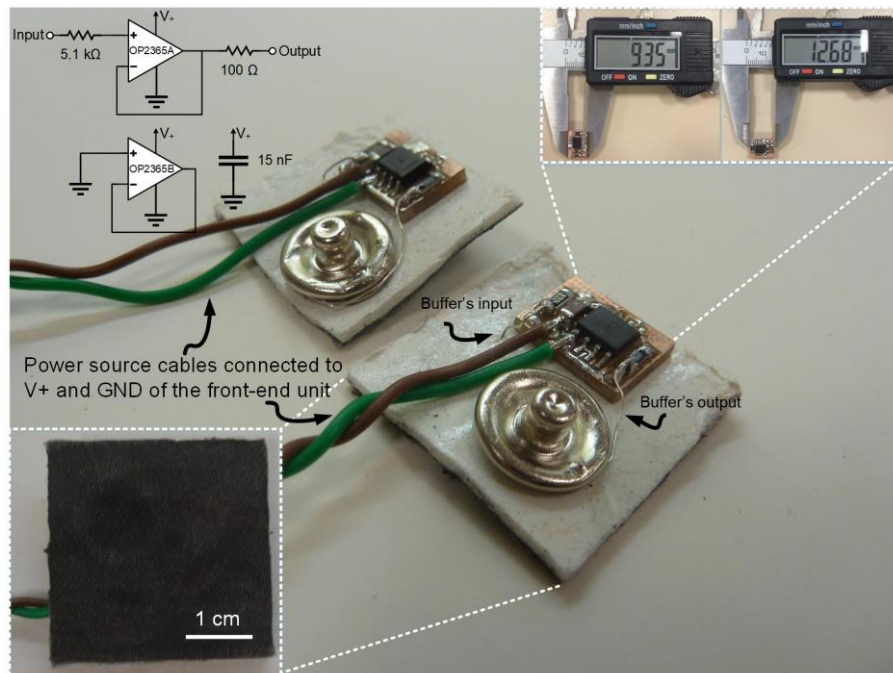


Figure 3.6. Fabric active electrode; zoomed-in shows a front-side of the electrode where the graphene-based textile electrode is and the size of the designed buffer circuitry with its component values.

### 3.2. System-level Architecture

Biopotential electrodes can be used to sense the weak, heavily noise-contaminated, and rarely deterministic physiological signals when fixed around the eyes. To identify the unique EOG patterns, first, the raw signal must be segregated from its noise components. Electromagnetic radiation, RF, mains hum,  $1/f$ , fluctuations in the electrode-skin interface, motion-related artifacts (e.g. cable or head movement), and other physiological signals such as cardiac (electrocardiography, ECG), neural (electroencephalography, EEG), and muscular (electromyography, EMG) are all considered as noise components in EOG [58]. Second, since EOG signals are small in magnitude (typically less than 500  $\mu\text{V}$ ) in order to be properly processed, amplification is needed. Third, the desired features are usually observed in the frequency range of DC to 10 Hz. All these requirements, in turn, necessitate a careful design of the biopotential amplifier.

Typical signal conditioning units for biopotential measurements include distinct hardware

and software stages. Having only a sophisticated analog front-end will create a massive electronic circuitry; which is hardly usable in wearable technologies. On the other hand, leaving all the filtering stages to the software, a complicated digital signal processing (DSP) algorithm will be required. Usually, the filtering algorithms should be run with feature extraction and classification algorithms simultaneously in real-time which makes schedulability tough for slow processors. Faster processors could be used to address this problem; however, this approach would also increase the circuit complexity and cost. Therefore, in the presented signal acquisition circuitry, a fine balance is maintained between the hardware and software sections to realize a robust, cost-effective system for point-of-care, wearable sensing.

The system-level block diagram of the developed prototype is shown in figure 3.7 along with a summary of component specifications in table I. In the analog front-end, the read-out circuitry receives the surface biopotentials from the graphene textile electrodes through sensor cables, which were twisted to reduce the magnetic pickups, and upon denoising with onboard filtering, signals are digitized in the microcontroller unit for further software filtering. Later on, data is sent to a personal computer for storage and real-time monitoring where it can be displayed through a graphical user interface (GUI) enabled by various platforms (e.g. LabVIEW®, Microsoft Excel®). For demonstration purposes and to simplify the circuit, we have focused on single-channel EOG acquisition and captured horizontal EMs which required bipolar montage of electrodes (i.e. two electrodes for differential amplification and one reference electrode). To amplify the weak and noisy surface biopotential signals, one of the key components in the analog front-end (figure 3.7) is the instrumentation amplifier (INA), which should reject the majority of the common-mode signals and must have high input impedance to minimize possible signal loss due to the skin-electrode contact impedance. The selected chip (INA128, Texas Instruments, USA) fulfills these requirements by having very high common-mode rejection ratio (CMRR) of 120 dB and input impedance of 10 GΩ. To significantly suppress the effect of high-frequency noise, an RC low pass filter (LPF) with a cut-off frequency of 780 Hz was included at the inputs. This is mainly because INA's CMRR is lower in high frequencies (e.g. according to INA128 datasheet CMRR drops to 80 dB in 1 kHz). Additionally, two antiparallel Schottky diodes supplemented the inputs to serve as further protection against electrostatic discharges and any other overvoltage peaks which could pose danger to the user and the circuitry.

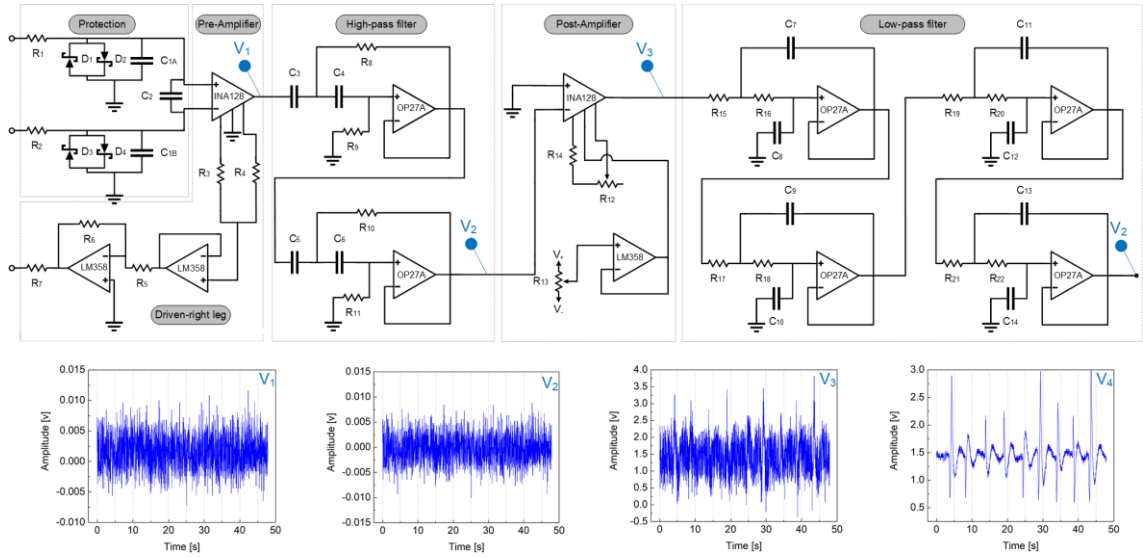


Figure 3.7. The hardware-level schematic of the analog section of the signal conditioning unit (frequency bandwidth: 0.3–10 Hz, adjustable gain: 600–4600 V/V) for the successful acquisition of the EMs, along with experimentally measured signals at the output of each block.

TABLE I  
COMPONENT VALUES AND SPECIFICATIONS FOR THE FRONT-END CIRCUITRY

| Sections              | Parts and Specifications  |
|-----------------------|---|
|                       | R <sub>1</sub> –R <sub>2</sub> (1 kΩ), R <sub>3</sub> –R <sub>4</sub> (2.2 kΩ), R <sub>5</sub> (10 kΩ),<br>R <sub>6</sub> –R <sub>8</sub> (390 kΩ), R <sub>14</sub> –R <sub>23</sub> –R <sub>24</sub> (100 Ω),<br>R <sub>9</sub> –R <sub>18</sub> (2.4 MΩ), R <sub>10</sub> (1 MΩ), R <sub>11</sub> (1.2 MΩ),<br>R <sub>15</sub> –R <sub>16</sub> (330 kΩ), R <sub>17</sub> (100 kΩ), R <sub>19</sub> (56 kΩ),<br>R <sub>20</sub> (1.4 MΩ), R <sub>21</sub> (12 kΩ), R <sub>22</sub> (470 kΩ) |
| EOG front-end circuit | R <sub>12</sub> –R <sub>13</sub> (potentiometer): 1 kΩ<br><br>C <sub>1A</sub> –C <sub>1B</sub> (1 nF), C <sub>2</sub> (100 nF), C <sub>3</sub> –C <sub>4</sub> (560 nF),<br>C <sub>5</sub> –C <sub>6</sub> (470 nF), C <sub>7</sub> –C <sub>8</sub> (270 nF), C <sub>9</sub> (150 nF),<br>C <sub>10</sub> (15 nF), C <sub>11</sub> (180 nF), C <sub>12</sub> (18 nF),<br>C <sub>13</sub> (680 nF), C <sub>14</sub> (68 nF)<br><br>D <sub>1</sub> –D <sub>6</sub> : 1N5819                     |
| Microcontroller       | ATmega328, ADC sampling frequency: 100 Hz, UART baud rate: 128000 b/s   |
| Power regulators      | UA79M05, KA7805 (Texas Instruments)   |

During measurements, an unpredictable DC baseline was observed in the EOG signal showed variations among different individuals. This offset variation is due to non-deterministic fluctuations in head shape, skin thickness, skin conductivity, skin moisture, electrode locations, ambient lighting [37] and overall mood of the users (e.g. tired, sleepy, just awaked) [115]. To reduce these anonymous, non-controllable parameters, some strategies were implemented.

First, the shifting resting potential (i.e. drift) was eliminated with the use of a 4<sup>th</sup> order Butterworth high-pass filter (HPF) based on Sallen-Key topology with a cut-off frequency at 0.3 Hz. In order to avoid op-amp saturation in the HPF stage, the gain of the pre-amplifier was kept low ( $\sim 10$  V/V). Second, a calibration procedure was implemented to configure the post-amplification stage gain and DC offset, both of which were designed to be variable within the range of 60-460 V/V and  $\pm 5$  V, respectively. Adding a specific DC voltage is primarily due to the requirements of the analog-to-digital converter (ADC) which accepts only positive values up to 5 V. Additionally, the option of adjusting gain and offset is instrumental for faster configuration of wearable EOG devices functioning on thresholding-based algorithms for automatic EM detection. The offset was achieved by a simple voltage divider connected to a buffer and instrumentation amplifier. The purpose of the buffer was to ensure that the reference pin of the INA was driven by low impedance. In order to further improve the CMRR and avoid potential dangers due to direct connection of the reference lead to the body, driven-right leg (DRL) circuit was designed and added to the system [22].

To limit the range of frequencies to 10 Hz a very sharp roll-off, 8th order, Butterworth LPF with Sallen-Key topology was implemented at the last stage before ADC which also served as an anti-aliasing filter prior to sampling. Additionally, placement of a sharp LPF at the last stage proved to significantly lower 50 Hz magnetic coupling noise compared to any other configuration. For all the filtering stages, op-amps (Op27, Analog Devices, USA) with low noise characteristics were selected; whereas, for the buffer stages, a general purpose op-amp (LM358, Texas Instruments, USA) was chosen. The circuit was realized in a printed circuit board (PCB) format with off-the-shelf surface mount components (SMD) and its operation was verified by using a multiple channel oscilloscope to monitor the output of each block. EOG waveforms after passing through the pre-amplification (V1), HPF (V2), post-amplification (V3) and LPF (V4) stages are plotted in figure 3.7; where the offset and gain were set to  $\sim 1.5$  V and  $\sim 4200$  V/V, respectively.

For achieving digitization, built-in ADC of the microcontroller unit ( $\mu$ CU) having 10-bit resolution was used with a sampling rate of 100 Hz based on the Nyquist theorem, and clamp diodes were placed at the ADC's input to limit the input signal amplitude within a specific voltage range. The digitized signal was then smoothed by Kolmogorov



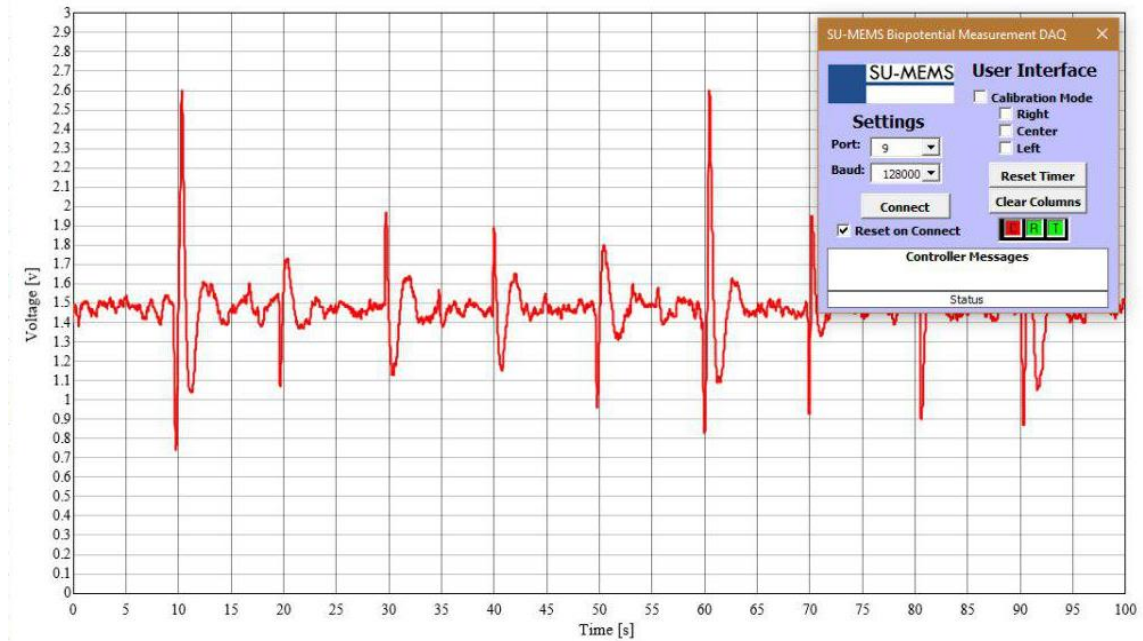


Figure 3.7. EOG signal after smoothing in the  $\mu$ CU which is displayed in real-time through the preliminary Microsoft Excel-based GUI.

Zurbenko filter, which executes a rolling average for eliminating the small variations in the output EOG due to stabilization of the eyes (i.e. microsaccades). In order to be monitored in real-time, data was continuously streamed via USB port to a computer with UART baud rate of 128000 b/s and displayed in Microsoft Excel through the use of a software add-in tool (PLX-DAQ, Parallel Inc., USA) illustrated in figure 3.8. Power consumption was estimated as  $\sim 39$  mW, which was supplied by a  $\pm 9$  V DC source.

By the advancements in this work, front-end circuitry modified to better address the wearability concerns of the system. The 4 generations of the biopotential acquisition circuitry are shown in figure 3.9 which starts from a simple breadboard prototype to a pocket worn battery-powered circuit. One of the points which were missing in the previous acquisition units before the 4<sup>th</sup> one was the fact that they were not designed to be battery-powered and data communication with a general purpose computer on them was by the means of a USB cable. So afford has been placed to fulfill these drawbacks.

Therefore, a better miniaturized and compact circuitry was designed (figure 3.10). Compared with the previous design, the new one has 2<sup>nd</sup> step and 4<sup>th</sup> step Butterworth HPF and LPF with cut-off frequencies of 0.5 Hz and 10 Hz, accordingly both based on



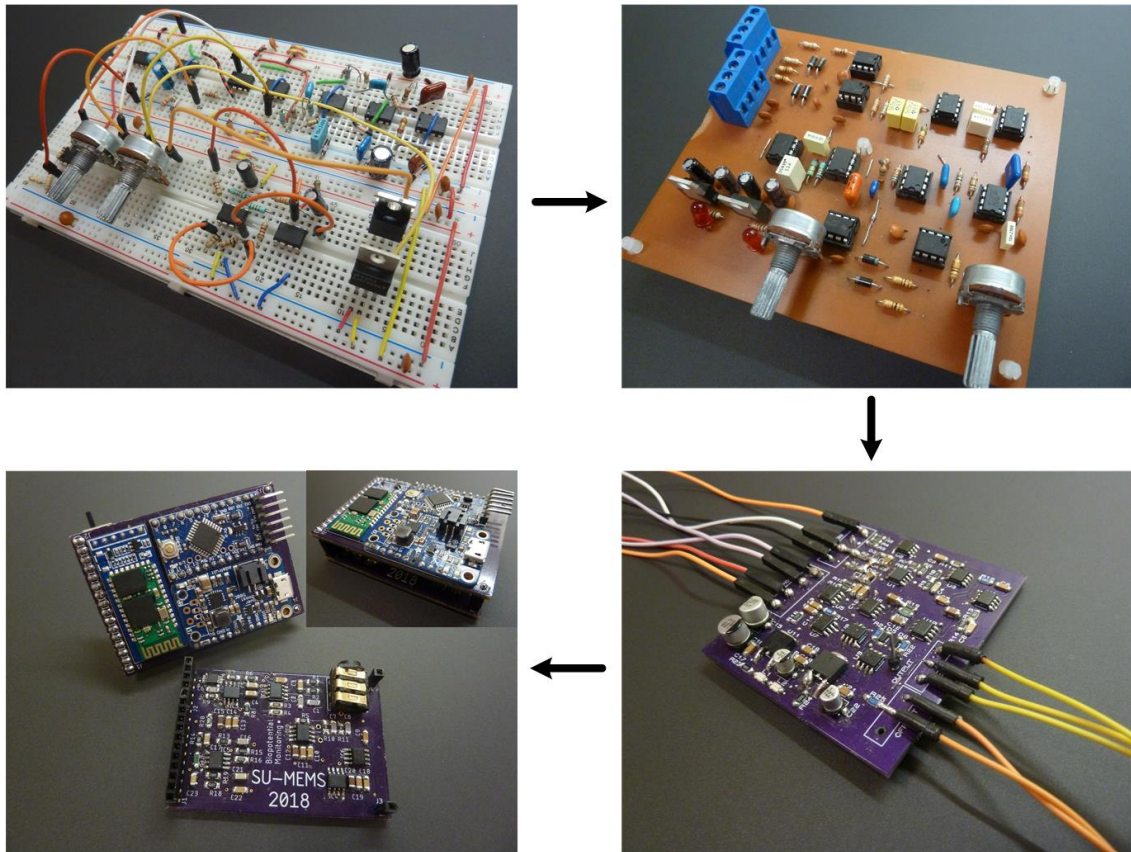


Figure 3.9. 4 generations of designed hardware's for EOG acquisition starting from breadboard prototype, to single-sided PCB, to SMD components assembled PCB, and the final smaller version where microcontroller is also mounted on the system.

Sallen-Key topology. The selected INA (INA122, Texas Instruments, USA) is designed for battery-powered applications with the capability of running with a single supply. Similarly, the other op-amps are also changed with single-supply rail-to-rail ones (OPA2365, Texas Instruments, USA). The volume for adjusting the gain in post-amplification stage replaced by a digitally programmable voltage divider (MAX5421, Maxim, USA) so that it can be configured in software level through GUI. As a usual practice in portable devices nowadays, a Lithium-ion/polymer battery having 3.7v and 500 mAh chosen to supply the system. The battery charger manager circuitry and DC to DC boost converter are based on MCP73831 (Microchip, USA) and TPS61090 (Texas Instruments, USA), accordingly. In order to split the regulated 5V, a rail-splitter (TLE2426, Texas Instruments, USA) was used. It is basically a glorified voltage divider, so it replaces the resistors in the simple resistor-divider but unlike a simple resistor divider, though, it has some buffering circuitry inside to prevent it from becoming unbalanced. The main problem with the power splitters usually is that they can handle

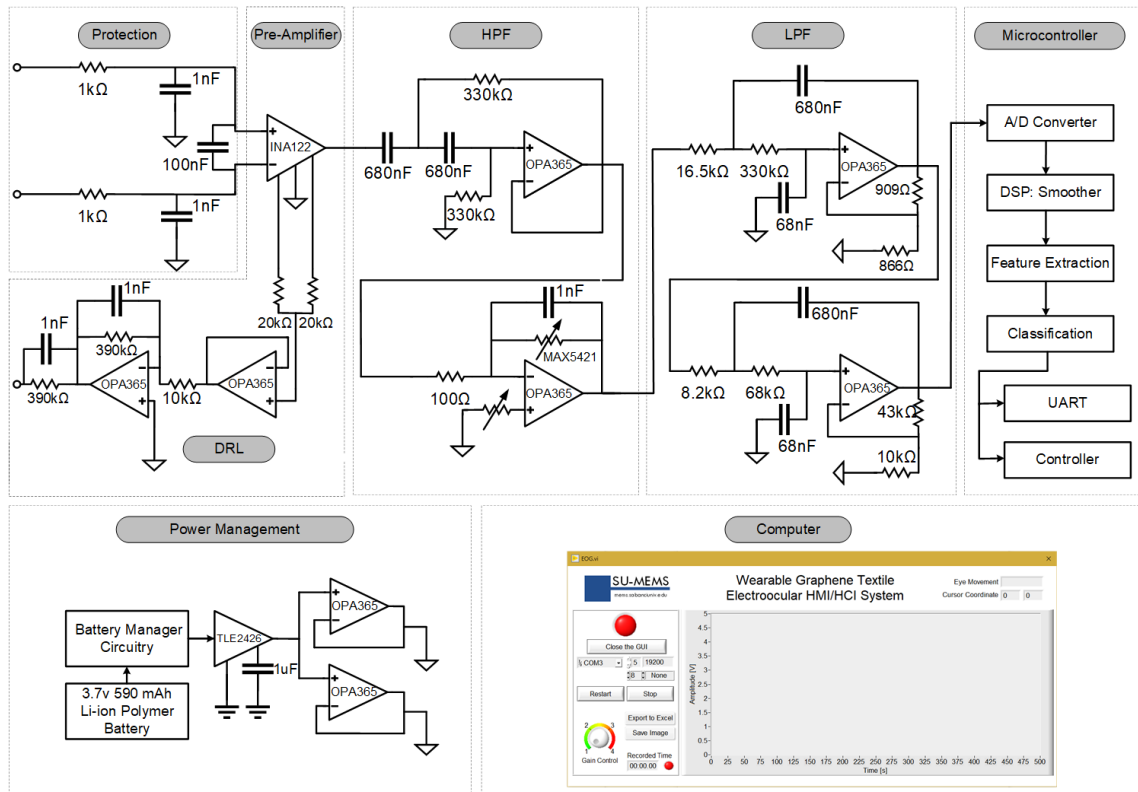


Figure 3.10. The hardware-level schematic of the portable, battery-powered, EOG acquisition unit including onboard filtering and gain stages, power management section, microcontroller unit to process and stream data wirelessly to a computer, and a costume-design GUI in LabVIEW.

only 20-40 mA of current. Although in this application the circuit will not draw too much current but standing in the safe side additional buffers are used which can handle current in the range of hundreds of milliamps. For streaming data to a computer, a popular off-the-shelf Bluetooth module (HC06) is used and in the receiving-end, a custom-designed GUI based on LabVIEW is prepared which enabled mainly for easier operation, calibration, gain manipulation, event monitoring in compared with the previous preliminary one.

### 3.3. Experimental Performance Characterization

In order to verify the feasibility of the developed graphene textile electrodes in sensing electrooculogram, they were benchmarked against the clinical standard, pre-gelled

Ag/AgCl electrodes (Ref 2228, 3M™Red Dot™, USA) in three different sets of experiments.

### **3.3.1. Simultaneous Experiments from Single Subject**

In the first set of experiments, both graphene-coated textile and standard Ag/AgCl electrodes were positioned side-by-side, around the same location on the subject's forehead and tested simultaneously. EOG recordings from a total of 8 voluntary participants (2 female, 6 male) aged between 20 and 30 years (average = 25, SD = 3.2 years) were acquired in this study. Among the participants, four had vision problems (three participants had myopic, one had hyperopic eyes) of which two were wearing glasses during the experiments and the remaining two were asked to remove glasses or contact lenses during the EOG recordings. The rest of the volunteers were healthy and without any obvious signs of eye or vision conditions.

Participants were instructed to sit and face straight ahead a pre-determined center point (primary position) from which two other points were located ~ 72 cm to the left and right sides, such that the participants had to make ~ 30° saccadic EMs when asked to look towards these gaze points. Prior to the experiments, the participants were informed of the three-stage testing protocol (figure 3.11) which consisted of several horizontal saccadic movements, fixations, and voluntary blinks. The subjects were asked to avoid spontaneous (involuntary) blinks as much as they could; but if such cases occurred, the trial was not interrupted. Therefore, the recorded electrooculograms inevitably contain waveforms due to involuntary blinks which are for example identified in figures 3.14a and 3.14b and as appeared in participants 1, 3, and 5 in figure 3.12.

The first stage begins with a voluntary blink while maintaining eyes in the primary position, then a levoversion (left gaze) is performed where both eyes are moved to the left and fixed for 10 s, after which eyes are brought back to the primary position. Continuing with the second stage, a dextroversion (right gaze) is performed where eyes are now moved from the primary position to the right and fixed for 10 s, and subsequently returned to the primary position. The third stage begins with a blink followed by swift left and right movements (levoversion and dextroversion) without waiting on the sides

(i.e. no fixations), and the protocol is concluded by a blink as eyes return to the primary position. Throughout this thesis, saccadic moves with a fixation duration on sides are called “slow movements” and moves with no fixation on the sides are called “swift movements”. To clearly distinguish the different EM patterns from the recorded electrooculograms, the duration between subsequent movements was maintained at approximately 10 s by timing the participant and alerting with a beep sound for each movement. Additionally, the ambient lighting was adjusted not to be dark nor bright. During experiments, it was observed that the best patterns are induced when volunteers have taken enough rest and without bearing physical tiredness. Therefore, morning to noon period was chosen for the recording of the EOG activity. During the pre-determined gaze points as defined in the protocol.

Total of five rounds of recording sessions were performed on each subject. In the first round, the system was calibrated wherein an offset was added to the signals by directing the participant to hold their gaze at the center point and fixate eyes at the primary position.

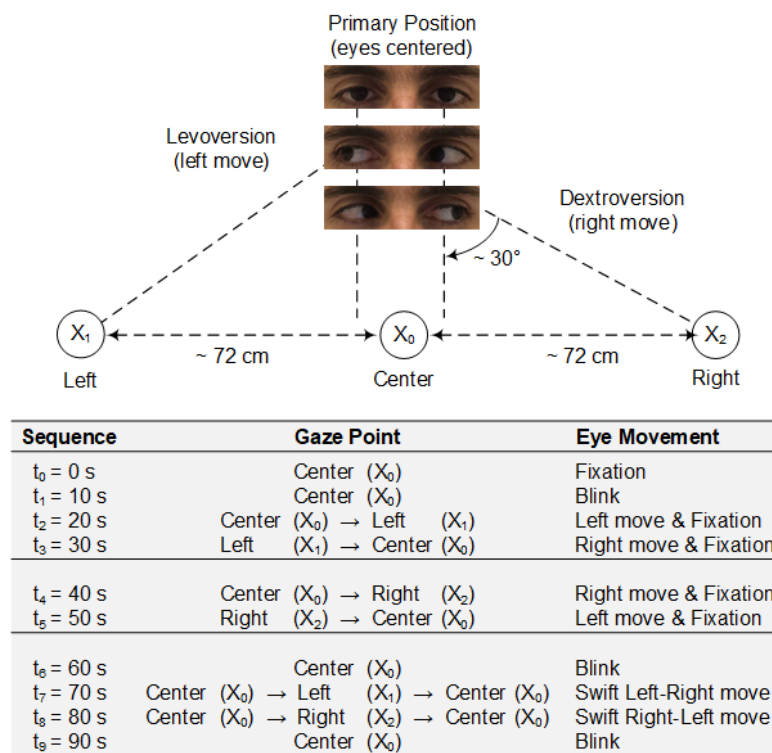


Figure 3.11. Schematic diagram showing the position of the eyeballs with respect to specific gaze points located straight ahead in the center ( $X_0$ ), towards the left ( $X_1$ ) and right ( $X_2$ ), along with a tabular summary of the sequence of EMs in the three-stage testing protocol.

Once the desired offset was ensured, the gain level was adjusted by taking only voluntary blinks into consideration. During the calibration procedure, EOG signals from most participants were acquired with the same gain configuration, with the exception of subjects having hyperopic or myopic eyes who displayed a clear difference in the gain requirement. This variation is attributed to higher EOG potentials in myopic eyes compared to non-myopic eyes and lower in hyperopic eyes [116]. After the calibration, two practice runs were performed to determine if the subject mastered the protocol or not. Upon successful completion of the practice runs, two more rounds were conducted where the electrooculograms were actually recorded for further analysis. To quantify the overlap between signals obtained with the graphene textile dry electrodes and conventional Ag/AgCl wet electrodes, the built-in linear correlation function of MATLAB® (Mathworks, USA) was used. The correlation coefficients (table II) between signals recorded from eight participants during the two trials reveal the maximum correlation of 87% for a 95 s recording (trial 1— participant 2) and a minimum of 57% for an 87 s recording (trial 2—participant 4). Average of signal correlations for eight participants was 79% and 78% in trial 1 and trial 2, with a standard deviation of 6% and 10%, respectively.

For each participant, the set of signals that displayed the highest overlap were plotted in figure 3.12a, along with detailed comparison and interpretation of different EMs in a representative EOG recording obtained with graphene textile (figure 3.12b) and Ag/AgCl (figure 3.12c) electrodes from the first participant. Comparison of the recorded signals reveals that the characteristic EOG biopotentials due to horizontal saccadic EMs including levoversion and dextroversion; as well as, voluntary blinks and fixations were accurately captured by both electrodes. Correlation of the signals for the entire recording period of 100 s illustrate high overlap of 86% which demonstrates the functionality of the developed graphene textile electrode in EOG measurements.

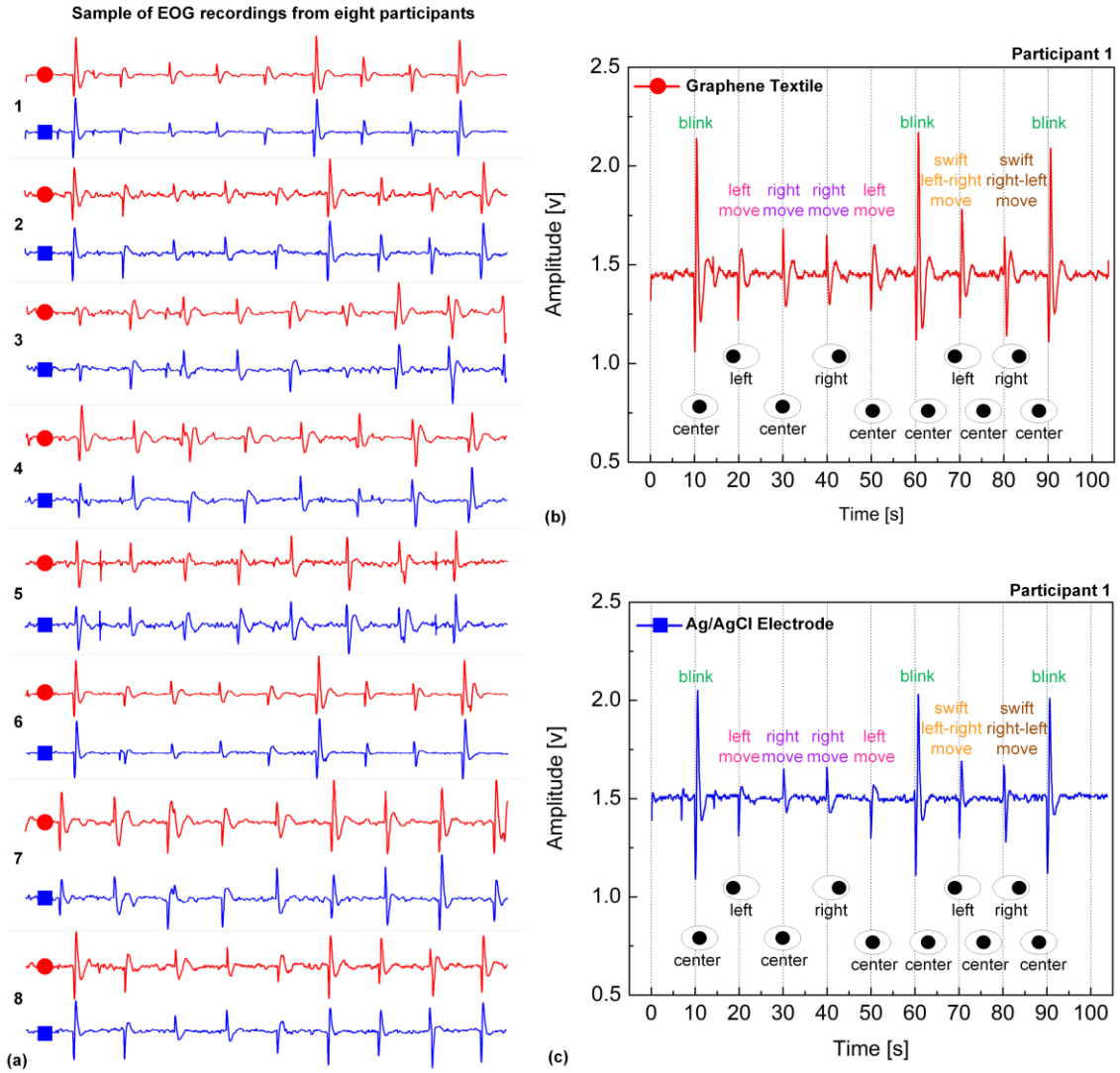


Figure 3.12. (a) Subset of EOG recordings obtained using graphene textile and Ag/AgCl electrodes that displayed the highest correlation among the 2 trials on 8 different participants; (b) zoom-in EOG signals showing the unique EM patterns acquired from participant 1 using graphene textile electrodes; and (c) Ag/AgCl electrode.

TABLE II  
CORRELATION COEFFICIENTS BETWEEN SIGNALS ACQUIRED WITH GRAPHENE TEXTILE AND AG/AGCL ELECTRODES

| Subjects           | Correlation Coefficient |                | Duration (s) |
|--------------------|-------------------------|----------------|--------------|
|                    | <i>Trial 1</i>          | <i>Trial 2</i> |              |
| 1                  | 0.86                    | 0.85           | 100          |
| 2                  | 0.87                    | 0.84           | 95           |
| 3                  | 0.71                    | 0.78           | 90           |
| 4                  | 0.73                    | 0.57           | 87           |
| 5                  | 0.76                    | 0.86           | 90           |
| 6                  | 0.77                    | 0.78           | 100          |
| 7                  | 0.82                    | 0.71           | 90           |
| 8                  | 0.80                    | 0.82           | 95           |
| Average            | 0.79                    | 0.78           | 93           |
| Standard Deviation | 0.06                    | 0.10           | 4.90         |



### 3.3.2. Simultaneous Experiments from Two Subjects

In biopotential measurements, the actual location of the electrodes placed on the body has a direct effect on the characteristics of the acquired signal, as such the second experiment

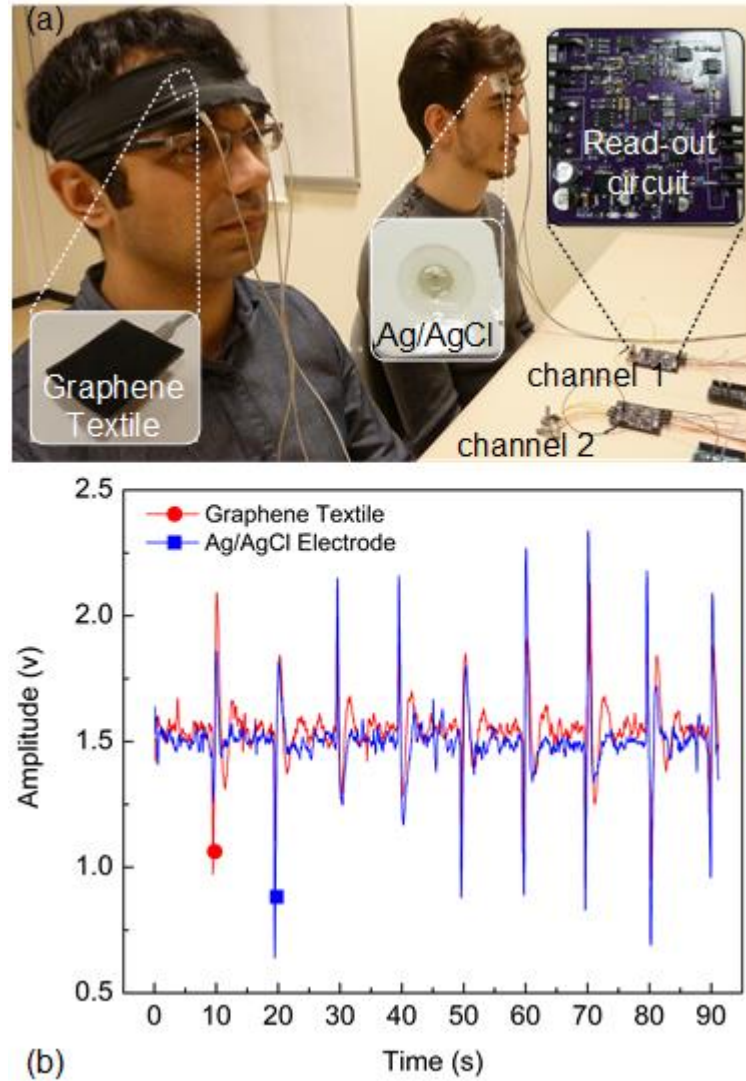


Figure 3.13. (a) Experimental setup showing the simultaneous acquisition of electrooculograms from two subjects where one is attached with graphene textile electrodes and the other with Ag/AgCl electrodes; (b) plot of the recorded signals.

was designed to keep the position of the electrodes constant during EOG acquisition. However, it is physically not possible to place two different electrodes on the same point at the same time. Therefore, two participants who displayed the highest overlap coefficients in the first set of trials (same person, different locations) were selected for a simultaneous demo (figure 3.13a) where graphene textile electrodes were attached to one participant, while the other person had pre-gelled, Ag/AgCl electrodes. This experimental

configuration allowed simultaneous acquisition of EOG biopotentials from two channels using the custom-designed read-out circuit (figure 3.13a inset). The participants were again instructed with a beeper to synchronize their eye activities and asked to follow the same protocol that included saccadic EMs, fixations, and blinks. Even though graphene textile and Ag/AgCl electrodes were positioned on two different persons which inevitably introduces physiological variations and therefore differences in individual biopotentials, the recorded electrooculograms were in very good agreement and exhibited 73% correlation over a duration of 90 s (figure 3.13b).

### 3.3.3. Asynchronous Experiments from Single Subject

In the third evaluation experiments, locations of both embedded textile electrodes and wet electrodes kept the same, and measurements were taken at different times but from the same location with two different types of electrodes. Signals from the forehead of the participant 1 were first collected using the headband without any prior skin preparation. After mounting, 5-minute wait period was allocated to allow electrode stabilization [117].

Approximately 10 minutes after completion of the first measurement, textile electrodes were removed and Ag/AgCl electrodes were placed around the same spots and the second part of the experiment was performed. Figures 3.14a and 3.14b display the recorded electrooculogram signals from the smart headband and Ag/AgCl electrodes respectively, along with the interpretation of the performed EMs. For both electrode types, the same

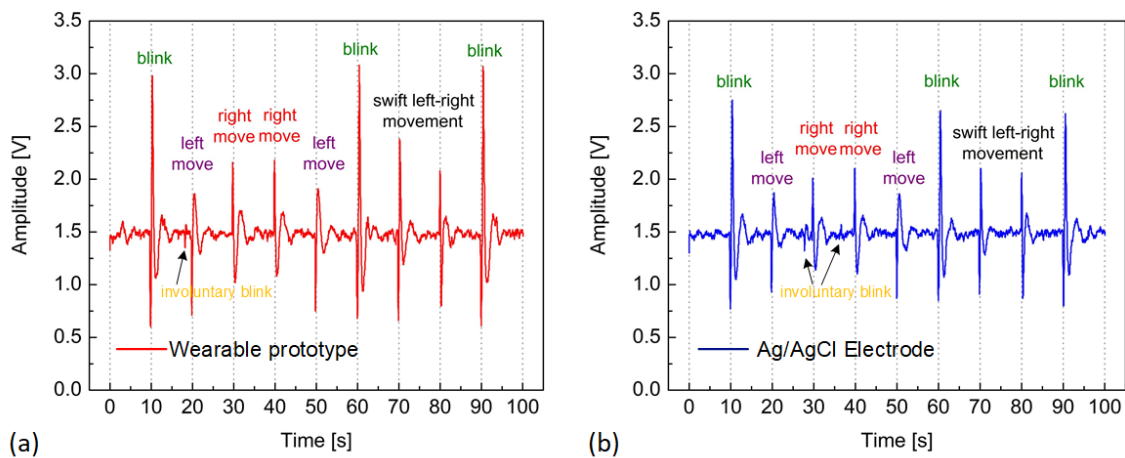


Figure 3.14. EOG signal acquired from (a) the developed smart headband showing the unique EM patterns, and (b) Ag/AgCl electrodes.



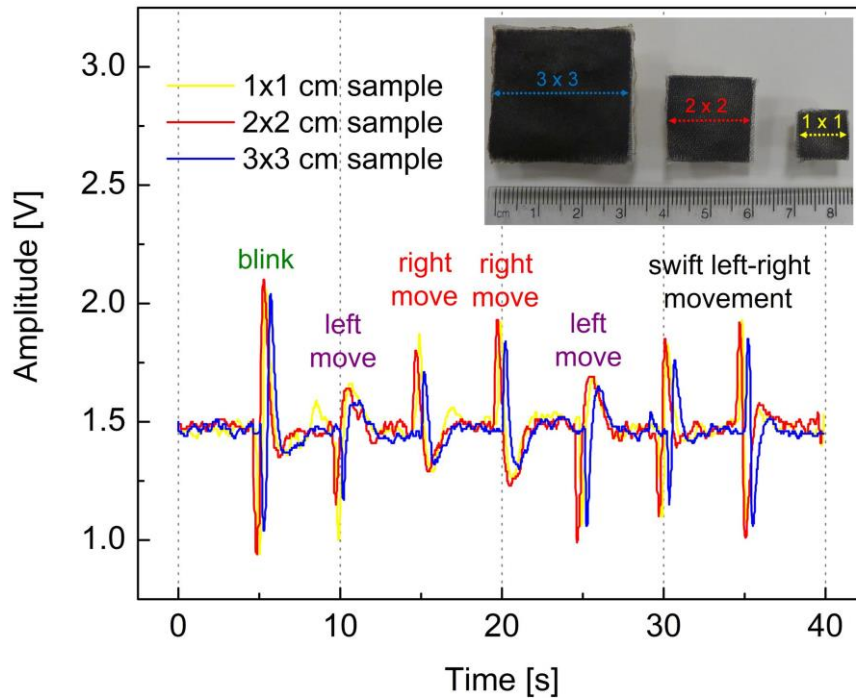


Figure 3.15. The plot of EOG signals acquired from three different sizes of graphene textile electrodes; inset shows an image of the fabricated electrode samples.

acquisition unit was used and gain and offset values were kept constant for a better comparison of the recorded signals (i.e.  $\sim 4400$  V/V and 1.5 V). The overlap between obtained signals was calculated to have a correlation of 91.3% for the entire measurement period of 100 seconds which was the highest obtained correlation in the reported three evaluation experiments and thus stresses out the fact that slight changes in the electrode positioning significantly affects electrooculograms.

### 3.3.4. Electrode Size Tuning Characterization

In experiments mentioned earlier, slight differences in amplitude are observed between the signals recorded with graphene textile and Ag/AgCl electrodes due to mismatches in measurement conditions and electrode characteristics. Additionally, as graphene textile electrodes are manually-sized, this causes inevitable size variations from textile to textile, and also between textiles to Ag/AgCl electrodes, which can potentially affect the signal quality. With automated handling, closer size match between electrodes could be achieved. To better assess the effect of electrode size on the recorded electrooculograms, we have fabricated and tested electrodes of varying contact areas of  $1 \text{ cm}^2$ ,  $4 \text{ cm}^2$ , and  $9$

cm<sup>2</sup>. Figure 3.15 shows the acquired waveforms from different electrode sizes as a result of saccadic EMs and blinks. It has been suggested that textile electrodes with larger contact areas could achieve better signal quality (i.e. less noise contamination) due to the smaller skin-electrode impedance [118]. In our measurements, this phenomena was not apparent due to sharp onboard filtering, and minimal to virtually no respiration-related change in contact conditions in EOG, unlike typical ECG applications. Moreover, while there are slight differences in the waveforms recorded by different electrode sizes, this is attributed primarily due to mismatches in experimental conditions and amplitude variations due to electrode size were observed to be insignificant, which is also in alignment with earlier studies on ECG [119].

## CHAPTER IV

### **REMOTE CONTROL OF OBJECTS FOR HCI/HMI APPLICATIONS**

A quick visual analysis of the recorded EOG waveforms shows that there is an exclusive signal pattern for each and every defined EM. These patterns mainly alter in shape, magnitude, and duration. By hard-coding, the unique signature of each EM pattern into the software, automatic detection of EMs can be accomplished. To do so, a unique sequential, multi-step, fixed thresholding algorithm was developed. Although other algorithms such as hidden Markov model and dynamic time warping has been reported to be instrumental with classifying complex EMs [54, 55], thresholding-based algorithms are more popular for single-directional EMs due to (probably) their simplicity in implementation.

Figure 4.1 illustrates a summarized flowchart of the developed algorithm. The algorithm is responsible to implement the following tasks: 1) maintain synchronize with the GUI, 2) digitize the denoised signal, 3) normalize the data, 4) extract information and features from the signal, 5) compare the extracted data with the hard-coded patterns, 6) classify the signal, and finally, 7) the algorithm should generate control signals according to specific application requirements (e.g. generating clock pulses or control comments). Since all of the mentioned tasks are “soft” real-time and they do not have critical deadlines, they can be scheduled by a periodic approach with the microcontroller's internal timer. During algorithm development, special emphasis was placed on avoiding the use of real-time operating system, or complicated DSP techniques, feature extraction or classification algorithms to ensure that the developed embedded “software” can operate on slow processing speeds (e.g. max ~20 MHz) and implemented on general purpose, small size, and low-cost microcontrollers.

A timer interrupt service routine is programmed to perform several tasks which include, triggering of an A/D conversion according to the desired sampling rate (e.g. 100 Hz), measuring the duration of potential EMs, running a time window and continuously checking and controlling the inputs and outputs (figure S1).

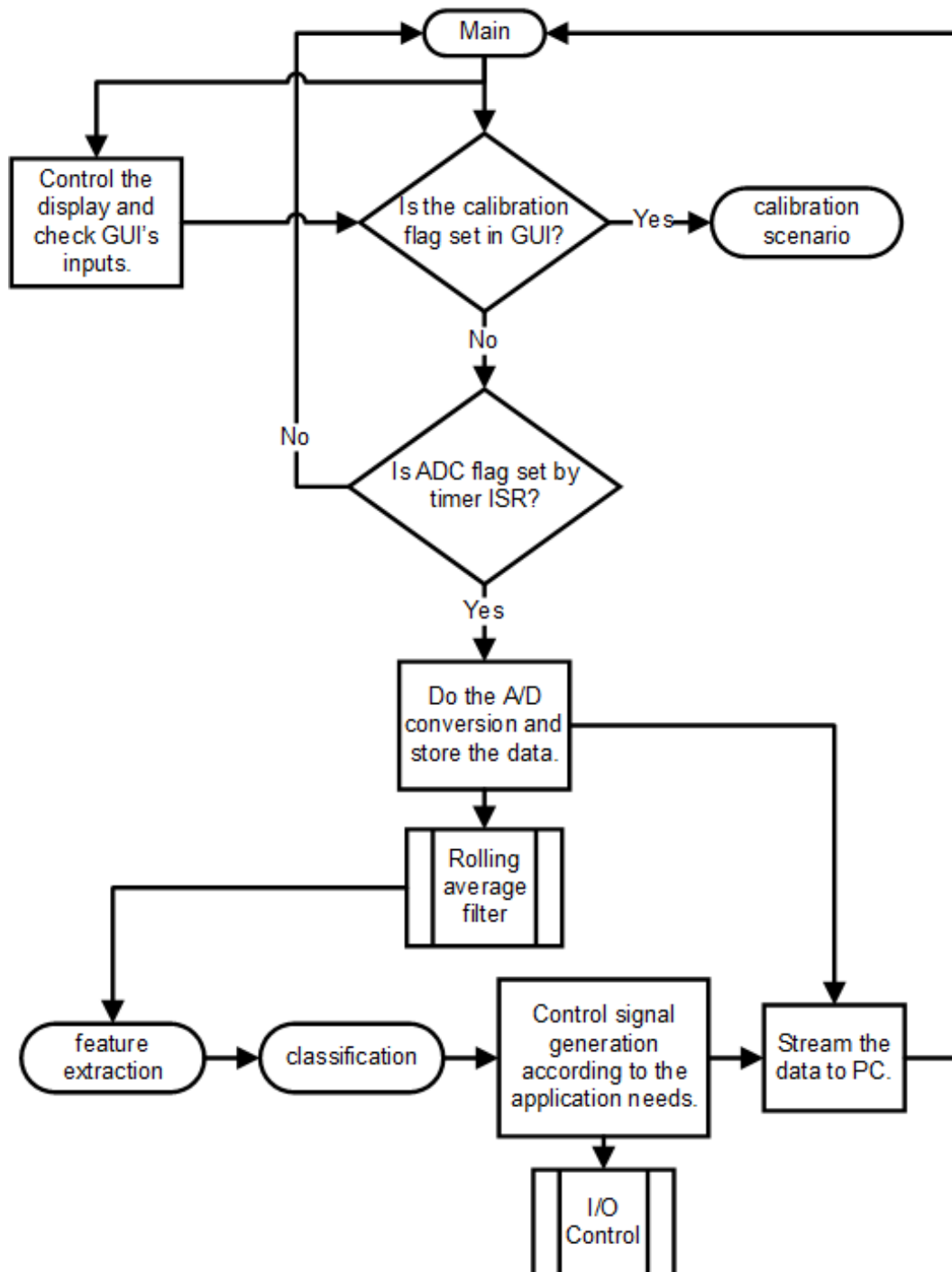


Figure 4.1. Summarized flowchart of the developed algorithm for automatic detection of blink along with four different saccadic EMs in single-channel forehead EOG.

## 4.1. Pattern Recognition

In order to construct a pattern model, one of the primary tasks is to regularly track the location of the real-time EOG signal which may include various EMs (figure 4.2a). Five threshold levels were defined and named as “up margin” (UM), “baseline up-margin” (BUM), “baseline”, “baseline down-margin” (BDM) and “down margin” (DM) (figure 4.2b). These threshold lines along with the duration and peak to peak amplitude of defined EMs are measured and hardcoded to the system in advance during the calibration session.

In the literature, most calibration methods either adjust thresholds at the software level and leaves hardware-level parameters untouched or, the operator adjusts signals at the hardware level according to the software threshold needs and always leave software parameters constant. Here, we do a mixture of both where the system is calibrated during training sessions with the addition of an offset to the signals by directing the participant to hold their gaze at the central point and fixate eyes at the primary position. The baseline value should guarantee the signal to be in the positive domain below 5 V level; here it is fixed at 1.5 V. Once the desired offset was ensured, several EMs of each type were performed so that the gain level could be adjusted accordingly to prevent output saturation.

Meanwhile, at the software level thresholds for UM and DM are configured based on several constraints. First, blinks, swift moves, and right gaze must pass through and intersect the UM but left gaze must not. Second, all moves must pass through and intersect DM but right gaze must not. Here, UM and DM were found as 2.1 V and 1 V, respectively. Third, BUM and BDM levels with respect to the baseline were selected according to baseline fluctuation; which through measurements was determined to be  $\pm 0.1$  V. During experiments there was no need to re-adjust BUM and BDM, and the artificial baseline set at the beginning was hardly changed during weeks of experiments. However, especially in long-term use, variation of signal amplitude due to environmental, physiological or physical factors such as feeling of tiredness or change in skin-electrode impedance could be critical and require recalibration of gain and offset parameters.

## 4.2. Feature Extraction

In feature extraction (figure S2), right after normalizing the signal using a rolling average filter, which is implemented for minimizing the effect of stabilization phenomena of fixation [120], if the signal appears to have a large value than UM, the system will label the location of it as “up”, whereas if it lies in between BUM and BDM the location will be as designated as “center” and, if the data value is less than DM, the system will name the location of the signal as “down”. The location operator will not be changed if the signal is in between UM and BUM, or DM and BDM, to avoid oscillation of location operator in critical cases near margins. If the location operator changes, a flag will be set to alert the algorithm to implement the necessary actions in the classification section.

While the algorithm detects the defined EMs, it must also avoid detection of undefined EMs and response as one of the defined patterns. For instance, spontaneous or reflex blinks (which can have several shapes, durations, or amplitudes depending on the context), or small degree saccadic EMs (mainly resembling left/right moves but with a smaller magnitude may occur during office activities like reading or writing), and must be excluded from detection. Additionally, the main parameter which distinguishes the swift left-right move and different types of blinks from each other is their amplitude levels [121]. Therefore, measurement of the signal amplitude is critical for reliably constructing the pattern model.

## 4.3. Classification

In case of a flag alert for a signal location change, the system enters the classification section (figures S3 and S4); where the algorithm tracks the signal that occurred to identify its pattern. The volunteer blink complex (figure 4.2b) first changes its location from centre to down (stage 1), then returns to the centre (stage 2), then rises to up (stage 3), and eventually returns to primary central position (stage 4) with the following of an undershoot [121]. As soon as the signal enters stage 1 (marked as (1) in figure 4.2b), a counter starts keeping the time and stops when the signal reaches stage 4 (marked as (2)

in figure 4.2b). The interval between time 1 and 2 is measured as the signal duration and it must be lower than a set threshold.

Swift left-right gaze (figure 4.2c) and the volunteer blink patterns are nearly identical in terms of the locations at when a change in signal pattern occurs. Therefore, the

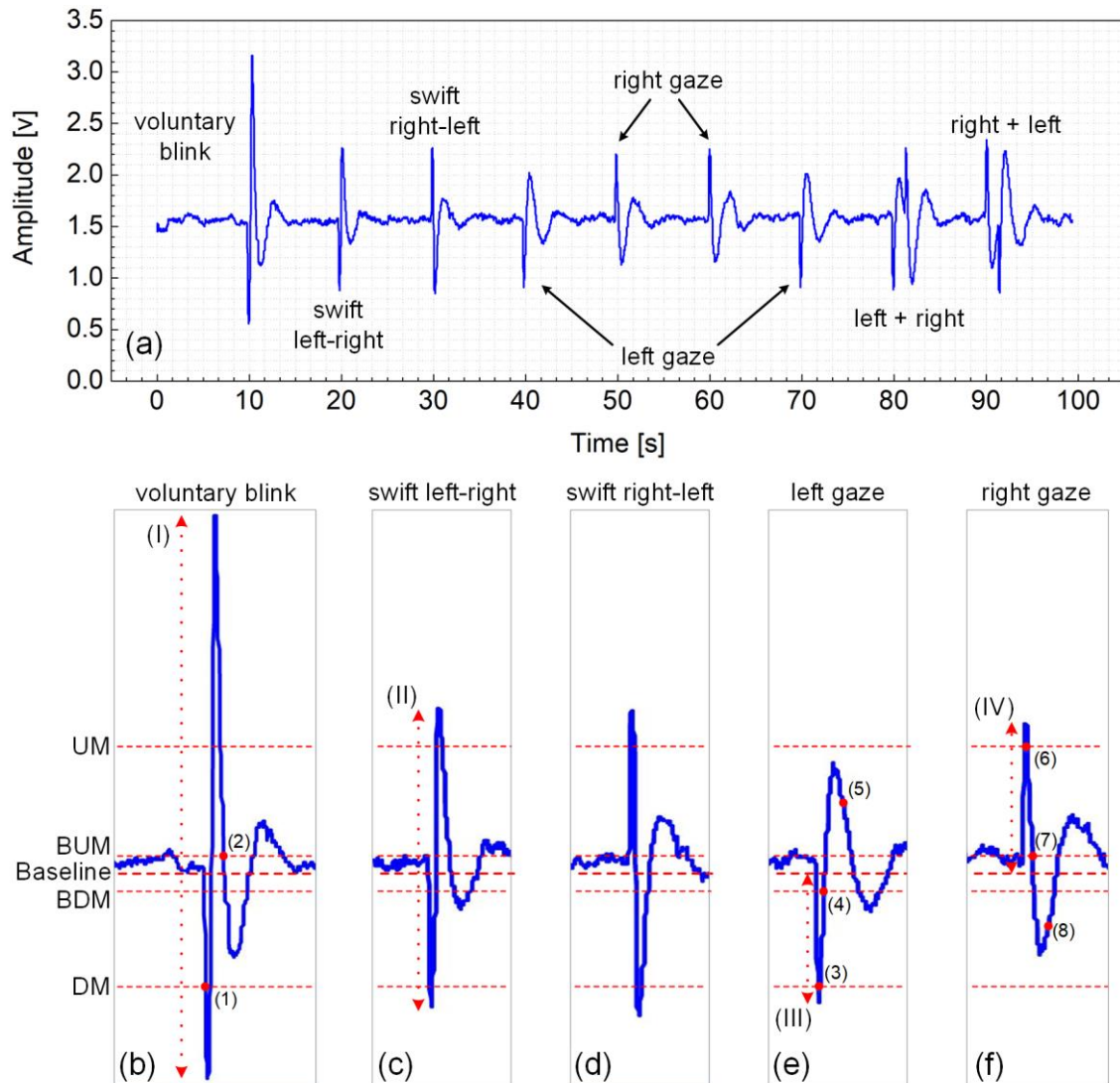


Figure 4.2. (a) EOG trace showing the different types of auto-detected EMs by the proposed algorithm, zoom-in images of the five exclusive signal patterns corresponding to (b) voluntary blink; (c) swift left-right saccadic gaze; (d) swift right-left saccadic gaze; (e) left gaze; and (f) right gaze. The labels “UM” (up margin), “BUM” (baseline up margin), “BDM” (baseline down margin), and “DM” (down margin) represent the critical threshold levels. The notations (I) to (IV) stand for amplitudes of blink, swift left-right, left and right movements, respectively; and the labels (1) to (8) correspond to data points between which the duration is measured.

stage indicator for a swift left-right gaze moves like the stage variable of a volunteer blink, but with a significantly different amplitude. Its amplitude (noted as “II” in figure 4.2c) must be lower than its threshold and definitely, it is smaller than the threshold introduced for the blink amplitude (noted as “I” in figure 4.2b). Swift right-left gaze (figure 4.2d) signal changes its pattern opposite to the behaviour of a blink, where it first starts by rising to up position (stage 1), then returns to center (stage 2), then falls down (stage 3), and finally returns to center (stage 4) with the following of an overshoot. Since the unique pattern of swift right-left gaze differs it from all other movements, no other threshold is required for building its model.

Left gaze (figure 4.2e) first changes its location from center to down (stage 1) and then returns to center (stage 2) with following of an overshoot which never reaches the UM level. The algorithm for detecting left gaze relies on two timer counters, one counts the duration between “3” and “4” which should not pass a specific threshold, and the other is a countdown timer which gives the system a short duration to check and find if the signal goes to “up” location or not. The same detection system stands for the right gaze (figure 4.2f), which is essentially the reverse pattern of a left gaze. In the right gaze signal first rises up (stage 1) and then returns to center with a following of undershooting which must not intersect DM. Before detecting the pattern as a valid EM, its timer counters control the duration threshold between its stage 1 and 2, and its down counter provides an interval to check if the signal will pass UM or not.

Then, the algorithm computes the amplitude of the signal and compares it with its respective threshold value. For calculating the amplitude of the pattern, ultimate high hillock and ultimate low valley points are found out by continuously comparing the maximum and minimum data values with each other in a pre-defined time window. If the system detects a specific attribute of the EOG signal as one of the five defined EMs, it will initiate a unit pulse with different amplitude for each detected pattern. Additionally, GUI displays the detected EM's name, amplitude, and duration. Moreover, a buzz sound is generated by the GUI to alert the operator of an EM detection event.



## 4.4. Proof of Concept Experiments

Rather than testing the feasibility of the developed wearable EM detector on a single application, we decided to investigate the fundamental needs of different applications in multiple testing scenarios.

### 4.4.1. Blink Controlled Clock Transaction Experiment

The first experiment involves translating volunteer blinks into a trail of pulses that can be used to trigger output commands for various control purposes such as selecting a button or implement a switching action in an HCI interface. The blink command was instructed by the participant according to a prescribed protocol which involved blinking at different time intervals; including 2.5, 5, 10, 15 s intervals such that the duty cycle of generated pulses was kept constant at  $\sim 50\%$ , and once 15 s interval was reached the blink repetitions were sequentially decremented back to 2.5 s (figure 4.3). During 5 minutes of continuous experimentation, 40 blinks occurred, where the algorithm was able to detect all and achieved a perfect success rate (SR) of 100%.

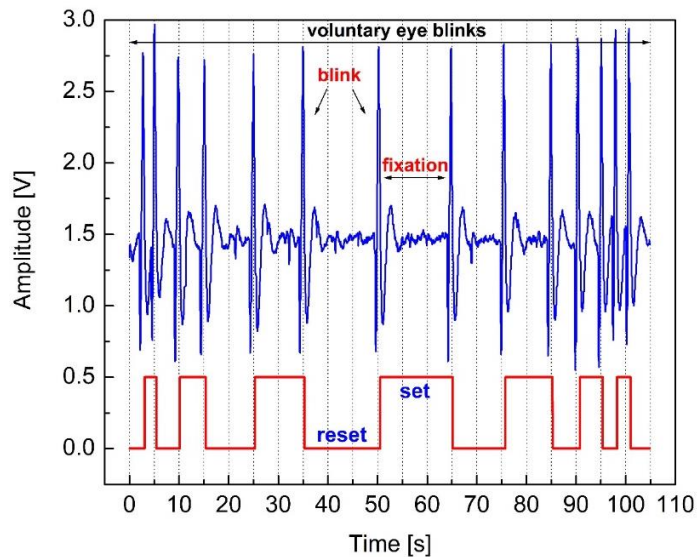


Figure 4.3. EOG signals acquired with the smart garment (blue trace), where the recorded signal includes several voluntary blink patterns which can be translated into a series of digital pulses (red trace) to effectively implement blink-controlled clock transitions in real-time for enabling switching requirements of HCI devices. Detection of the spontaneous blinks that occurred in the 22nd, 33rd, and 69th seconds were avoided.

#### **4.4.2. Pattern of “8” Trace Experiment**

In the second experimental scenario, LEDs were turned on sequentially in a 5 by 5 LED matrix to trace certain patterns like “S”, “5”, and “8” (figure 4.4). The swift EMs cause the “on-LED” (i.e. lit-up LED) to move in horizontal directions while slow horizontal saccades move the on-LED in the vertical direction and voluntary blinks cause flashing of the on-LED. As illustrated in figure 4.2a, if right after hearing the alert for detection of a slow left or right gaze, the user follows a natural flow and makes a reverse gaze to bring eyes back to the primary position, the induced signal complex will be a combination two gazes. In most cases, this return does not satisfy the conditions to be considered as a separate left or right gaze and therefore will not be detected by the algorithm. However, after hearing the alert if the gaze is fixated on the sides longer than a natural detection, the algorithm will categorize the second gaze as a valid EM. For the particular switching applications like this one or the 3<sup>rd</sup> experiment, this could be problematic because the second eye gaze, that is also a reverse of the first one, will cause the on-LED to return to its previous position and effectively cancel the intended move. Thus, for the demonstrated application, the extra measures were implemented at the software level to eliminate the second EM in case of its detection.

#### **4.4.3. Long term Durability Experiment**

Another important consideration for successful development of wearable electronics is their long-term performance which is fundamentally related to both hardware and algorithm design. In order to test the long-term performance and reliability of the developed algorithm, a multi-segment EOG, which included performing of various EMs and indoor activities was conducted for a duration exceeding 1 hour. Figure 4.5 illustrates the induced electrooculograms along with the unit pulses generated by the algorithm to identify the detected EMs. In the first and last segments of this experiment, a similar protocol of the one introduced in figure 3.11 which the volunteer had mastered earlier, was carried out. In the second, fourth, fifth, and seventh segments a single type from one of the defined EMs was performed; namely, they are voluntary blink, swift left, swift right, slow left, and slow right movements, respectively. In the third segment, an English text having 32 lines was read from a laptop display. In the sixth segment, the participant

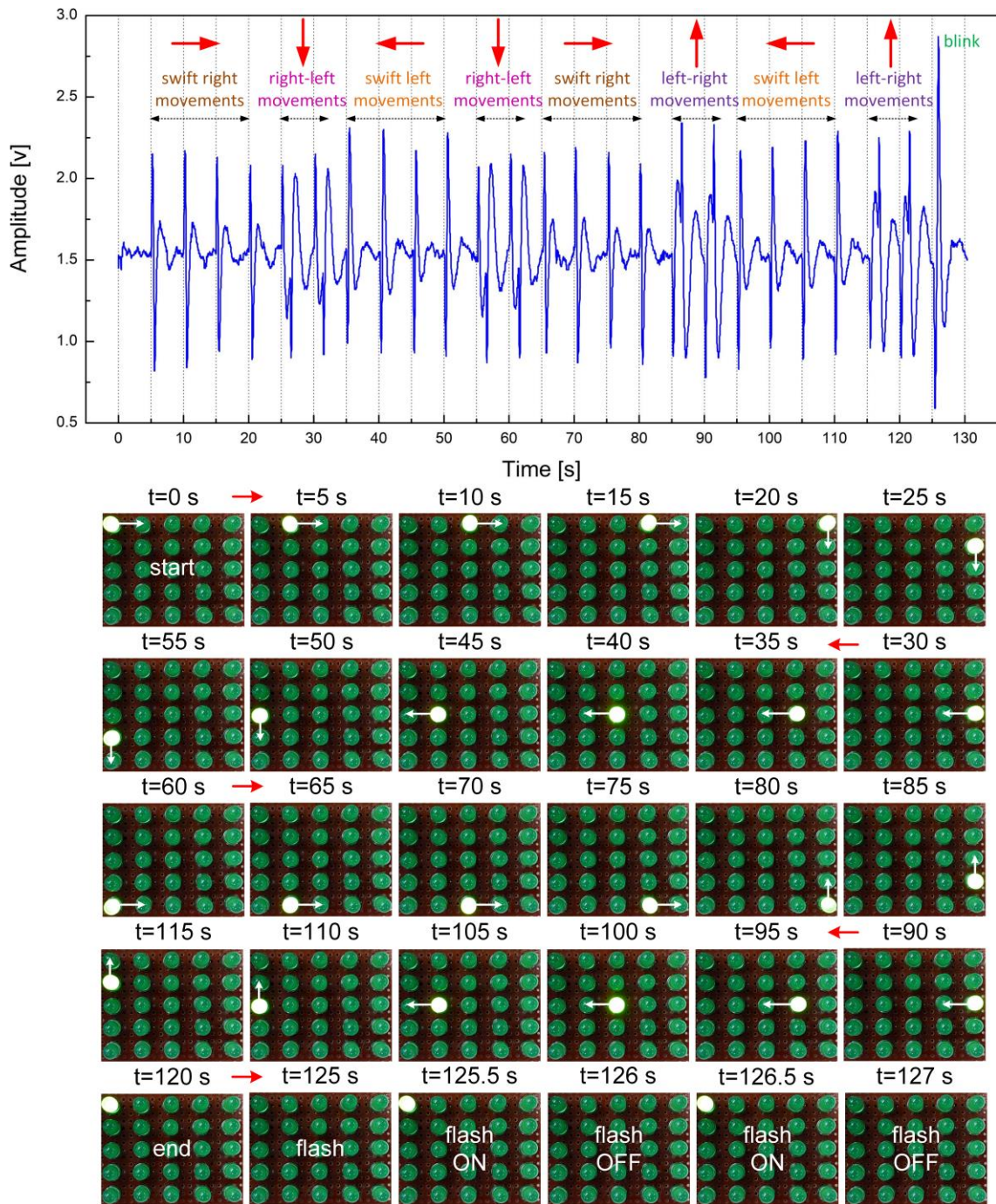


Figure 4.4. Plot of the induced EOG signal with inserted interpretations for each movement and their issued direction changes, which are used to control an array of LED by turning them on sequentially to trace a pattern of “8”.

was reading text on a smartphone, watching short video clips and messaging. In the eighth segment, the participant was requested to relax and stare at a single point and, in the tenth segment, the same task was implemented with eyelids closed. Finally, in between some of the segments, the participant was asked to watch a neutral video.

Table III summarizes the performed activities including their duration, the total number of EMs (either voluntary, reflex, or spontaneous), and the algorithm's SR in EM detection throughout for each segment and for every EM. While performing this experiment the participant's eyes were being recorded so that later on, the recorded EMs could be tracked visually to verify the performance of the algorithm in automatic detection of EMs. Additionally, the threshold calibration was conducted only once at the beginning of the 1-hour EOG session.

Throughout the 1-hour-long EOG session, the algorithm correctly detected 70 voluntary blinks out of 72 (SR = 97.2%), 60 left gazes out of 62 (SR = 96.7%), 50 right gazes out of 61 (SR = 81.9%), 58 swift left gazes out of 59 (SR = 98.3%), and 64 swift right gazes out of 64 (SR = 100%), also it successfully avoided detection of 462 spontaneous and reflex blinks out of 507 occurrences (SR = 91.1%).

Data indicates that most of the miss detected EMs were involuntary blinks which were interpreted by the algorithm as slow left moves. The number of spontaneous blinks occurred while watching a video (~20 minutes) is more than double of the other segments combined and also most of the misdetection of spontaneous blinks happened while watching the video. The higher number of involuntary blinks while watching the video is attributed to reflex blinks. In this context, the reflex is not due to an external signal stimulus rather we are referring to the visual stimulus in the break of senses or luminance change during the video [122]. The reason for larger number of miss detected involuntary blinks could be due to the difference in the overall shape and magnitude of reflex blinks compared to spontaneous blinks [121], wherein our experiments the reflex blinks were observed to resemble a slow left gaze pattern and were misinterpreted by the algorithm. This could be addressed simply in calibration session by increasing the threshold value for the left gaze.

An interesting observation was made for the recorded EOG signals when eyes were closed. Simple visual comparison of the induced signals in segment 8 (i.e. eyes open and staring at a single point) with those of segment 10 (i.e. eyes closed and at the primary position) reveal that variations and magnitudes of electrooculogram when eyes are closed are higher than the case where eyes are open. This also suggests that the same calibration

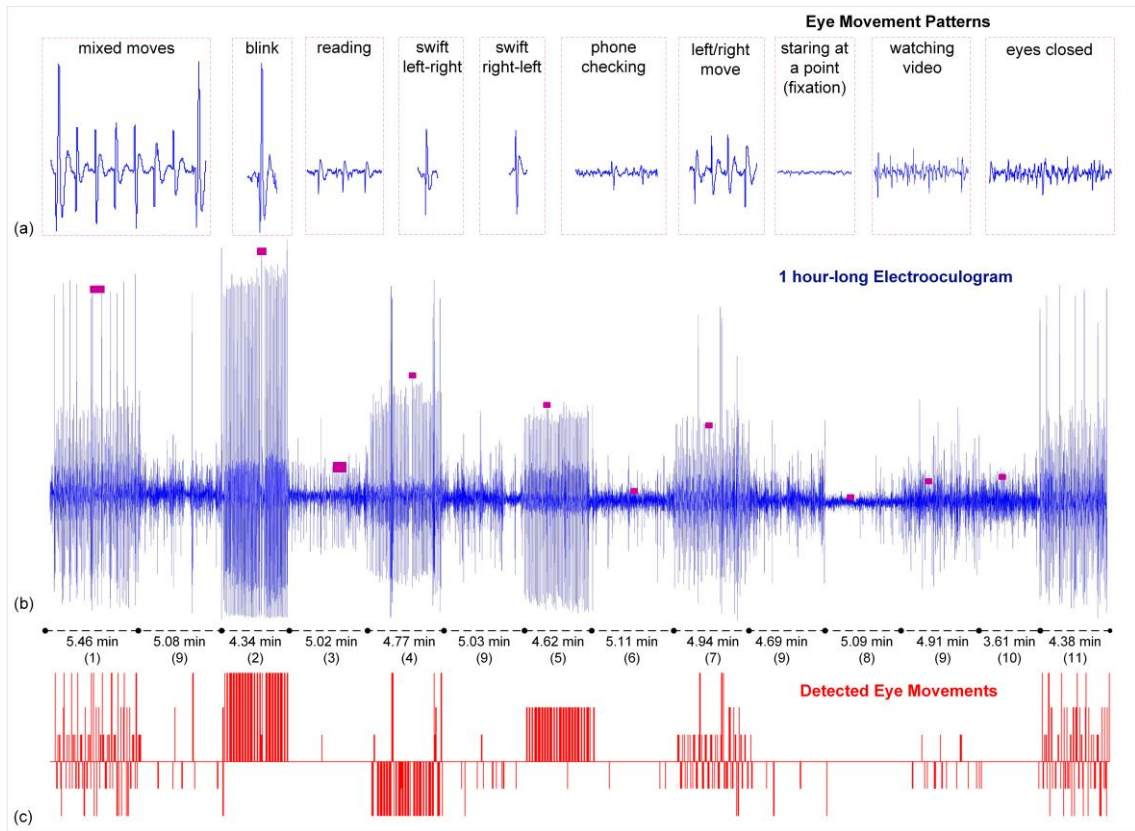


Figure 4.5. (a) Zoom-in samples from each performed activity (b) 1 hour-long electrooculogram (c) virtual unit pulses generated by the algorithm displaying different amplitudes according to the detected EMs. 0.1 V and 0.2 V pulses are for slow and swift right EMs, respectively; whereas, pulses with the same amplitude but with negative sign are indicators of slow and swift left EMs. Pulses with the highest amplitude correspond to the detection of voluntary blinks.

parameters cannot be used for detection of slow and/or swift saccadic EMs for cases when eyes are open versus closed. As for the reading activity, the recorded electrooculograms display 30 low-amplitude saccadic left moves due to focusing on different lines of the text while the algorithm successfully avoids their detection owing to the fact that left gaze pattern for saccadic moves was modeled for  $\sim 30^\circ$  displacements, not for smaller changes like  $\sim 10^\circ$  which typically occur while reading.

In the 1-hour EOG session, a decline in the SR from 97% (first segment) to 87.1% (last segment) is observed where both segments roughly contain the same number of EMs. The reason for the decline in SR is the high number of miss detection or completely missing



TABLE III  
TABULAR SUMMARY OF SUCCESS RATE OF THE AUTOMATIC DETECTION OF EYE MOVES IN DIFFERENT SCENARIOS IN 1-HOUR LONG EOG

| <b>activity</b>     | <b>1</b> | <b>2</b> | <b>3*</b> | <b>4</b> | <b>5</b> | <b>6</b> | <b>7</b> | <b>8</b> | <b>9</b> | <b>10</b> | <b>11</b> | <b>SR</b> |
|---------------------|----------|----------|-----------|----------|----------|----------|----------|----------|----------|-----------|-----------|-----------|
| <b>VB</b>           | C/T      | 10/10    | 47/47     | 3/4      | -        | -        | 3/3      | -        | 1/1      | -         | 6/7       | 97.2%     |
|                     | MD       | 0        | 0         | 1        | -        | -        | 0        | -        | -        | -         | 0         | 1         |
| <b>L</b>            | C/T      | 18/19    | -         | -        | -        | -        | 25/26    | -        | -        | -         | 17/17     | 96.7%     |
|                     | W        | 0        | 1         | -        | 1        | 3        | 3        | -        | 27       | 1         | 0         | 36        |
| <b>R</b>            | C/T      | 19/19    | -         | -        | -        | -        | 22/26    | -        | -        | -         | 9/16      | 81.9%     |
|                     | W        | 1        | 2         | 1        | 2        | -        | 4        | -        | 1        | -         | 0         | 11        |
|                     | MD       | -        | -         | -        | -        | -        | -        | -        | -        | -         | 4         | 4         |
| <b>SL</b>           | C/T      | 6/6      | -         | -        | 45/46    | -        | -        | -        | -        | -         | 7/7       | 98.3%     |
|                     | W        | 1        | -         | -        | 1        | -        | 2        | -        | 2        | -         | 1         | 7         |
| <b>SR</b>           | C/T      | 6/6      | -         | -        | -        | 51/51    | -        | -        | -        | -         | 7/7       | 100%      |
|                     | W        | 0        | -         | -        | 1        | 0        | 4        | -        | 1        | -         | 3         | 9         |
| <b>SB</b>           | MD/T     | 7/8      | 7/10      | 16/17    | 2/5      | 2/3      | 39/42    | 5/8      | 46/46    | 330/361   | 8/8       | 91.1%     |
| <b>Success Rate</b> |          | 97%      | 94.7%     | 94.1%    | 90.9%    | 98.1%    | 92.8%    | 86.6%    | 100%     | 91.4%     | -         | 87.1%     |

**C:** Correct detection, **T:** Total number of occurred moves, **MD:** Missing detection of occurred moves, **W:** Wrongly detect moves

*Note:* The **success rate (SR)** is defined as the percentage of the correct detection of occurred eye moves.

\* None of the small degree saccadic moves due to text's line change detected.

Definition of eye moves: **VB:** Voluntary Blink, **L:** Left move (both center to left side and right side to center movements), **R:** Right move (both center to right side and left side to center movements), **SL:** Swift left-right move without waiting for fixation at left side, **SR:** Swift right-left move without waiting for fixation at right side, **SB:** Spontaneous Blink

Definition of activity (minute): **1:** Mix of defined moves (5.46), **2:** Only blink (4.34), **3:** Reading (5.02), **4:** Only swift left-right move (4.77), **5:** Only swift right-left move (4.62), **6:** Phone checking (5.11), **7:** Only the left/right move with having fixation on sides (4.94), **8:** Staring at a single point (5.09), **9:** Watching video (5.08+5.03+4.69+4.91), **10:** Closed eyelids without moving eyes (3.61), **11:** Mix of defined moves (4.38)

of slow right gazes (nearly half) due to the insufficiency of their amplitude thresholds, indicating that the system needs recalibration session in long runs, which could be addressed by dynamic thresholding approaches [121].

#### **4.4.4. Eye Mouse Experiment**

In the fourth experiment, the developed embedded software for the second experiment modified to send x-y coordinates of the cursor to GUI. In the computer-end, the GUI calls Microsoft Windows User32.dll library and uses SetCursorPos and mouse\_event functions to control cursor movement and blink actions, respectively. The swift EMs facilitates horizontal cursor movements, whereas slow EMs control vertical directions and volunteer blink mimic the click action. When an EM occurs cursor starts to move in the defined direction with a configured speed until the arrival of another command or reaching to the edge of the display. For instance, it will be moving toward the left side with swift left EM and will be stopping if blink occurs and perform clicking. Some addition actions are also implemented in the software-level to ease the cursor control experience. For instance, when the cursor is in motion both swift EMs can stop the movement. Speed of the cursor, its initial starting point, and several other options are configurable in GUI settings. Figure 4.6. shows a demo with the developed eye mouse along with the recorded electrooculograms and their interpretation. The aim here is to first open Microsoft Word Office and virtual keyboard, then to write a word, and finally to stop the GUI. For the first trail, the speed kept slow, 1 pixel every 30 msec which is translated to 1 character every ~20 sec, but after a few exercises, the speed increased to 1 character per ~ 10 sec which is a fairly good speed for a thresholding-based algorithm approach having 100% accuracy in detection.

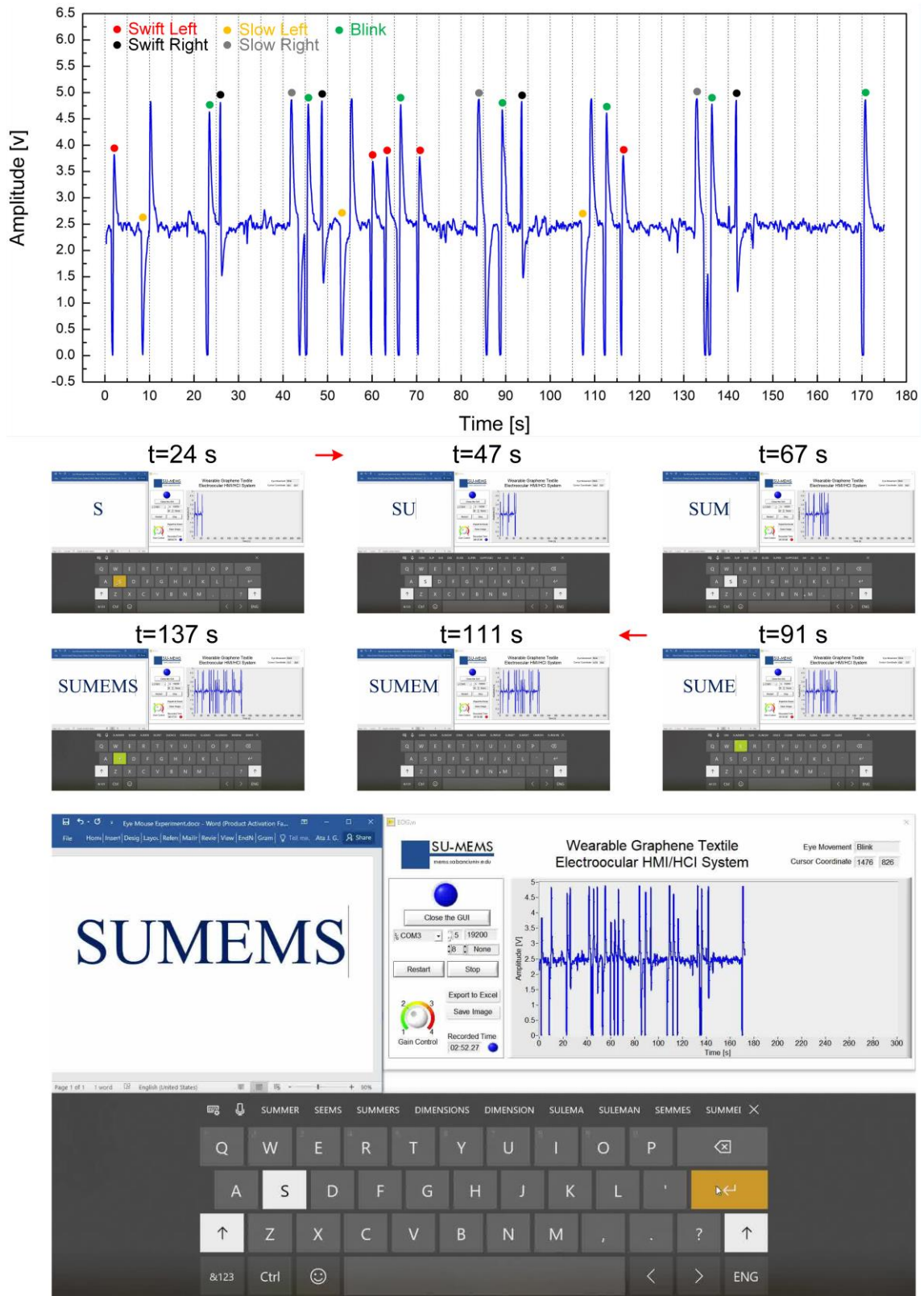


Figure 4.6. Plot of the induced EOG signal with inserted interpretations for each movement, which are used to mimic movements of a mouse cursor to write “SUMEMS”.



## CHAPTER V

### CONCLUSIONS

In contrast to well-established vision-based gaze tracking, EOG can be measured with body-worn sensors and can be implemented as an effective, cost-efficient, and low-power embedded system to estimate EMs. The approach involves recording under any light condition, and there is no influence from the presence of obstacles, even when the subject's eyes are closed. However, despite its merits, the number of studies on this subject is limited, and many topics and issues have been left unaddressed. Tackling its issues, it is expected that EOG becomes a useful source of communication in virtual reality environments and can act as a valuable communication tool for people with amyotrophic lateral sclerosis.

Following these lines, unlike traditional “wet” electrodes which profoundly hinder the development of wearable EOG sensors, this work employed, for the first time, the use of graphene-coated fabric electrodes and suggests them as suitable alternatives to overcome the limitations of the currently used conventional “wet” electrodes. In order to test the feasibility of the fabricated textile electrodes a total of 16 EOG recordings was performed which was acquired by simultaneous side-by-side placement of both electrodes on 8 different participants resulted in a signal correlation of ~ 80% on average and maximum of 87% for one participant. On the other hand, signals that were simultaneously acquired from 2 different participants where each wore a different type of electrode (i.e. either graphene textile or Ag/AgCl) displayed 73% correlation. Furthermore, the asynchronous recorded signal from a single participant revealed an excellent correlation of 91.3%. These experimental results verify the capability of graphene textile electrodes in accurately capturing the unique EOG patterns due to horizontal saccades, blinks and fixations with very high similarity to that of Ag/AgCl electrodes despite the physiological

differences between individuals, variations in contact conditions due to head shape, possible asynchronism of individuals while executing specific EM patterns, mismatches in measurement conditions and random noise components. Additionally, during the period of conducting the reported experiments which exceeded months, no significant performance changes were observed in the graphene textile electrodes. As for the biocompatibility of graphene, since graphene textiles do not require prior skin preparation and effectively touch only the outermost layer of the skin (i.e. stratum corneum, made up of several tens-of-microns-thick pile of dead cells), potential concerns on toxicity are alleviated as dermal administration of graphene has been reported to display minimal effect on the skin for moderate exposure durations and concentrations [100]. Owing to their accessible fabrication technique, graphene textile electrodes have the possibility and adaptability for mass manufacturing. Moreover, they display a high degree of flexibility and stretchability, and fabric materials offer comfortable interfaces for the body due to the elimination of the gel existing in wet electrodes. This assures the possibility of embedding the electrodes into garments and long-term usability of the EOG devices empowered wearable electronics based on graphene textile electrodes.

Wearable textile electronics and their application to biopotential signal acquisition is an emerging trend which grows steadily and shows large parallelism to the developments in the broader field of wearable or ubiquitous computing, which aims to develop and improve personalized routine health monitoring, rehabilitation devices, brain-computer interfaces, HCI/HMIs, prosthetics, and possibly many other applications that exploit biopotential feedback or control. The development of textile electrodes as a valid alternative to standard clinical electrodes is therefore critical due to their potential for seamless integration into daily clothing, the possibility of long-term functionality, breathability, stretchability, and for achieving “truly wearable” soft electronics. In this respect, textile electronics is a key technology enabler. Further developments from fundamental materials and system-level integration, including embedding of electronics, to strategies for compensating signal artifacts in dynamic operation and novel algorithms for a target application will determine the success and widespread use of wearable e-textile-based devices in the years to follow. With further development, seamless integration of graphene textiles with ordinary clothing and electronics it could be possible to revolutionize EOG applications including, monitoring of epileptic patients and driver drowsiness, diagnostic polysomnogram tests for sleep disorders, development of

wearable HCI.

Also in this work, a fully-wearable, smart headband was developed and its capability to auto-detect multiple EMs was demonstrated by system-level integration of graphene textiles with read-out electronics and classifier algorithms based on sequential, multi-step, fixed thresholding. With the approach provided in this study, a novel electrode placement for the forehead EOG was introduced whereby five different EM patterns could be detected only by a single channel read-out circuitry. The results presented in this work lay down the foundation of graphene textiles toward control applications specifically tailored to EOG-based HCI/HMI.

In summary, in this work we have shown that EOG provides several advantages over common systems based on video; in particular in terms of embedded implementation and long term recordings in daily life. However, in current work the information obtained from EOG remains coarse, the users are static, and signal processing is yet to be ideal in mobile scenarios which render future research directions to be carried on.

## BIBLIOGRAPHY

- [1] A. J. Golparvar and M. K. Yapici, "Wearable graphene textile-enabled EOG sensing," in 2017 IEEE SENSORS, 2017: IEEE.
- [2] A. J. Golparvar and M. K. Yapici, "Graphene-coated wearable textiles for EOG-based human-computer interaction," in 2018 IEEE 15th International Conference on Wearable and Implantable Body Sensor Networks (BSN), 2018: IEEE, pp. 189-192.
- [3] A. J. Golparvar and M. K. Yapici, "Electrooculography by Wearable Graphene Textiles," vol. 18, no. 21, pp. 8971-8978, 2018.
- [4] G. Acar, O. Ozturk, A. J. Golparvar, T. A. Elboshra, K. Böhringer, and M. K. Yapici, "Wearable and Flexible Textile Electrodes for Biopotential Signal Monitoring: A review," vol. 8, no. 5, p. 479, 2019.
- [5] A. J. Golparvar and M. K. Yapici, "Graphene Smart Textile-Based Wearable Eye Movement Sensor for Electro-Ocular Control and Interaction with Objects," vol. 166, no. 9, pp. B3184-B3193, 2019.
- [6] A. Duchowski, "A breadth-first survey of eye-tracking applications," vol. 34, no. 4, pp. 455-470, 2002.
- [7] N. N. Rommelse, S. Van der Stigchel, and J. Sergeant, "A review on eye movement studies in childhood and adolescent psychiatry," vol. 68, no. 3, pp. 391-414, 2008.
- [8] H. Chennamma and X. Yuan, "A survey on eye-gaze tracking techniques," 2013.
- [9] T. Eggert, "Eye movement recordings: methods," in Neuro-Ophthalmology, vol. 40: Karger Publishers, 2007, pp. 15-34.
- [10] C. H. Morimoto, and M. Mimica "Eye gaze tracking techniques for interactive applications," vol. 98, no. 1, pp. 4-24, 2005.
- [11] E. Whitmire et al., "EyeContact: scleral coil eye tracking for virtual reality," in Proceedings of the 2016 ACM International Symposium on Wearable Computers, 2016:

ACM, pp. 184-191.

[12] J. D. Ryan, L. Riggs, and D. McQuiggan, "Eye Movement Monitoring of Memory," no. 42, p. e2108, 2010.

[13] T. Pfeiffer, M. E. Latoschik, and V. R. Wachsmuth, "Evaluation of binocular eye trackers and algorithms for 3D gaze interaction in virtual reality environments," vol. 5, no. 16, 2008.

[14] D. Li, J. Babcock, and D. J. Parkhurst, "openEyes: a low-cost head-mounted eye-tracking solution," in Proceedings of the 2006 symposium on Eye tracking research & applications, 2006: ACM, pp. 95-100.

[15] D. Borghetti, A. Bruni, M. Fabbrini, L. Murri, and F. Sartucci, "A low-cost interface for control of computer functions by means of eye movements," Computers in Biology and Medicine, vol. 37, no. 12, pp. 1765-1770, 2007.

[16] L. R. Young and D. Sheena, "Eye-movement measurement techniques," American Psychologist, vol. 30, no. 3, p. 315, 1975.

[17] J. Malmivuo and R. Plonsey, "Principles and applications of bioelectric and biomagnetic fields," vol. 15, p. 12, 1995.

[18] V. Häkkinen et al., "The effect of small differences in electrode position on EOG signals: application to vigilance studies," vol. 86, no. 4, pp. 294-300, 1993.

[19] A. Lopez, F. Ferrero, M. Valledor, J. C. Campo, and O. Postolache, "A study on electrode placement in EOG systems for medical applications," in 2016 IEEE International Symposium on Medical Measurements and Applications (MeMeA), 2016: IEEE.

[20] S. N. Abbas and M. Abo-Zahhad, "Eye blinking EOG signals as biometrics," in Biometric Security and Privacy: Springer, 2017, pp. 121-140.

[21] R. Soundariya, and R. Renuga "Emotion recognition based on eye movement," vol. 11, no. 5 SI, pp. 38-44, 2017.

[22] J. G. Webster, Medical instrumentation application and design. John Wiley & Sons,

2009.

[23] M. F. Marmor, M. G. Brigell, D. L. McCulloch, C. A. Westall, and M. Bach, "ISCEV standard for clinical electro-oculography (2010 update)," *Documenta Ophthalmologica*, vol. 122, no. 1, pp. 1-7, 2011.

[24] R. Schleicher, N. Galley, S. Briest, and L. Galley, "Blinks and saccades as indicators of fatigue in sleepiness warnings: looking tired?," *Ergonomics*, vol. 51, no. 7, pp. 982-1010, 2008.

[25] W.-D. Chang, "Electrooculograms for Human–Computer Interaction: A Review," *Sensors*, vol. 19, no. 12, p. 2690, 2019.

[26] D. Beukelman, S. Fager, and A. Nordness, "Communication support for people with ALS," *Neurology Research International*, vol. 2011, 2011.

[27] S.-L. Wu, L.-D. Liao, S.-W. Lu, W.-L. Jiang, S.-A. Chen, and C.-T. Lin, "Controlling a human–computer interface system with a novel classification method that uses electrooculography signals," vol. 60, no. 8, pp. 2133-2141, 2013.

[28] X. Zheng, X. Li, J. Liu, W. Chen, and Y. Hao, "A portable wireless eye movement-controlled human-computer interface for the disabled," in *2009 ICME International Conference on Complex Medical Engineering*, 2009: IEEE.

[29] S. Aungsakun, A. Phinyomark, P. Phukpattaranont, and C. Limsakul, "Robust eye movement recognition using EOG signal for human-computer interface," in *International Conference on Software Engineering and Computer Systems*, 2011: Springer, pp. 714-723.

[30] A. Larson, J. Herrera, K. George, and A. Matthews, "Electrooculography based electronic communication device for individuals with ALS," in *2017 IEEE Sensors Applications Symposium (SAS)*, 2017: IEEE.

[31] Q. Ding, K. Tong, and G. Li, "Development of an EOG (electro-oculography) based human-computer interface," in *2005 IEEE Engineering in Medicine and Biology 27th Annual Conference*, 2006: IEEE, pp. 6829-6831.

[32] Y. Chen and W. S. Newman, "A human-robot interface based on

electrooculography," in IEEE International Conference on Robotics and Automation, 2004. Proceedings. ICRA'04. 2004, 2004, vol. 1: IEEE, pp. 243-248.

[33] Y. Kim, N. Doh, Y. Youm, and W. Chung, "Development of human-mobile communication system using electrooculogram signals," vol. 34, no. 4, pp. 245-250, 2001.

[34] A. López, P. Arévalo, F. Ferrero, M. Valledor, and J. Campo, "EOG-based system for mouse control," in SENSORS, 2014 IEEE, 2014: IEEE, pp. 1264-1267.

[35] A. B. Usakli, and S. Gurkan, "Design of a novel efficient human-computer interface: An electrooculogram based virtual keyboard," vol. 59, no. 8, pp. 2099-2108, 2009.

[36] S. Teja, S. S. Embrandiri, and N. Chandrathoodan, "EOG based virtual keyboard," in 2015 41st Annual Northeast Biomedical Engineering Conference (NEBEC), 2015: IEEE.

[37] R. Barea, L. Boquete, M. Mazo, and E. López, "System for assisted mobility using eye movements based on electrooculography," vol. 10, no. 4, pp. 209-218, 2002.

[38] A. Ubeda, E. Ianez, and J. Azorin, "Wireless and portable EOG-based interface for assisting disabled people," vol. 16, no. 5, pp. 870-873, 2011.

[39] L. Y. Deng, C.-L. Hsu, T.-C. Lin, J.-S. Tuan, and S.-M. Chang, "EOG-based Human-Computer Interface system development," Expert Systems with Applications, vol. 37, no. 4, pp. 3337-3343, 2010.

[40] D. Kumar and A. Sharma, "Electrooculogram-based virtual reality game control using blink detection and gaze calibration," in 2016 International Conference on Advances in Computing, Communications and Informatics (ICACCI), 2016: IEEE, pp. 2358-2362.

[41] D. Valeriani and A. Matran-Fernandez, "Towards a wearable device for controlling a smartphone with eye winks," in 2015 7th Computer Science and Electronic Engineering Conference (CEECE), 2015: IEEE, pp. 41-46.

[42] B.-S. Lin, P.-J. Wu, and C.-Y. Chen, "2D/3D-Display Auto-Adjustment Switch System," vol. 22, no. 3, pp. 799-805, 2017.

- [43] S. Venkataramanan, P. Prabhat, S. R. Choudhury, H. B. Nemade, and J. Sahambi, "Biomedical instrumentation based on electrooculogram (EOG) signal processing and application to a hospital alarm system," in Proceedings of 2005 International Conference on Intelligent Sensing and Information Processing, 2005., 2005: IEEE, pp. 535-540.
- [44] E. Moon, H. Park, J. Yura, and D. Kim, "Novel design of artificial eye using EOG (electrooculography)," in 2017 First IEEE International Conference on Robotic Computing (IRC), 2017: IEEE, pp. 404-407.
- [45] A. Banerjee, M. Pal, D. Tibarewala, and A. Konar, "Electrooculogram based blink detection to limit the risk of eye dystonia," in 2015 Eighth International Conference on Advances in Pattern Recognition (ICAPR), 2015: IEEE, pp. 1-6.
- [46] A. Banerjee and D. Tibarewala, "Electrooculogram based approach for prevention of dry eye condition in computer users," in 2016 IEEE First International Conference on Control, Measurement and Instrumentation (CMI), 2016: IEEE, pp. 503-507.
- [47] J. Yang, X. Su, D. Bai, Y. Jiang, and H. Yokoi, "Hybrid EEG-EOG system for intelligent prosthesis control based on common spatial pattern algorithm," in 2016 IEEE International Conference on Information and Automation (ICIA), 2016: IEEE, pp. 1261-1266.
- [48] C.-E. Kuo et al., "An EOG-based automatic sleep scoring system and its related application in sleep environmental control," in International Conference on Physiological Computing Systems, 2014: Springer, pp. 71-88.
- [49] S.-F. Liang et al., "Development of an EOG-based automatic sleep-monitoring eye mask," vol. 64, no. 11, pp. 2977-2985, 2015.
- [50] J. Arnin et al., "Wireless-based portable EEG-EOG monitoring for real time drowsiness detection," in 2013 35th Annual International Conference of the IEEE Engineering in Medicine and Biology Society (EMBC), 2013: IEEE, pp. 4977-4980.
- [51] J.-X. Ma, L.-C. Shi, and B.-L. Lu, "Vigilance estimation by using electrooculographic features," in 2010 Annual International Conference of the IEEE Engineering in Medicine and Biology, 2010: IEEE, pp. 6591-6594.



- [52] A. Bulling, J. A. Ward, H. Gellersen, and G. Tröster, "Eye movement analysis for activity recognition," in Proceedings of the 11th international conference on Ubiquitous computing, 2009: ACM, pp. 41-50.
- [53] R. OuYang, Z. Lv, and X. Wu, "An algorithm for reading activity recognition based on electrooculogram," in 2015 10th International Conference on Information, Communications and Signal Processing (ICICS), 2015: IEEE, pp. 1-5.
- [54] F. Fang and T. Shinozaki, "Electrooculography-based continuous eye-writing recognition system for efficient assistive communication systems," PloS one, vol. 13, no. 2, p. e0192684, 2018.
- [55] W.-D. Chang, H.-S. Cha, S. H. Kim, and C.-H. Im, "Development of an electrooculogram-based eye-computer interface for communication of individuals with amyotrophic lateral sclerosis," Journal of neuroengineering and rehabilitation, vol. 14, no. 1, p. 89, 2017.
- [56] K.-R. Lee, W.-D. Chang, S. Kim, and C.-H. Im, "Real-time "eye-writing" recognition using electrooculogram," IEEE Transactions on Neural Systems and Rehabilitation Engineering, vol. 25, no. 1, pp. 37-48, 2016.
- [57] A. Bulling, D. Roggen, and G. Tröster, "Wearable EOG goggles: Seamless sensing and context-awareness in everyday environments," vol. 1, no. 2, pp. 157-171, 2009.
- [58] S. Yao and Y. Zhu, "Nanomaterial-enabled dry electrodes for electrophysiological sensing: A review," vol. 68, no. 4, pp. 1145-1155, 2016.
- [59] L.-D. Liao, I.-J. Wang, S.-F. Chen, J.-Y. Chang, and C.-T. Lin, "Design, fabrication and experimental validation of a novel dry-contact sensor for measuring electroencephalography signals without skin preparation," vol. 11, no. 6, pp. 5819-5834, 2011.
- [60] J. Löfhede, F. Seoane, and M. Thordstein, "Textile electrodes for EEG recording—A pilot study," vol. 12, no. 12, pp. 16907-16919, 2012.
- [61] J.-C. Chiou et al., "Using novel MEMS EEG sensors in detecting drowsiness application," in 2006 IEEE Biomedical Circuits and Systems Conference, 2006: IEEE,

pp. 33-36.

[62] W. Uter and H. Schwanitz, "Contact dermatitis from propylene glycol in ECG electrode gel," vol. 34, no. 3, pp. 230-231, 1996.

[63] Y. M. Chi, T.-P. Jung, and G. Cauwenberghs, "Dry-contact and noncontact biopotential electrodes: Methodological review," vol. 3, pp. 106-119, 2010.

[64] E. Spinelli, M. Haberman, P. García, and F. Guerrero, "A capacitive electrode with fast recovery feature," vol. 33, no. 8, p. 1277, 2012.

[65] S. M. Lee, J. H. Kim, H. J. Byeon, Y. Y. Choi, K. S. Park, and S.-H. Lee, "A capacitive, biocompatible and adhesive electrode for long-term and cap-free monitoring of EEG signals," vol. 10, no. 3, p. 036006, 2013.

[66] P. Griss, H. K. Tolvanen-Laakso, P. Merilainen, and G. Stemme, "Characterization of micromachined spiked biopotential electrodes," vol. 49, no. 6, pp. 597-604, 2002.

[67] L.-S. Hsu, S.-W. Tung, C.-H. Kuo, and Y.-J. Yang, "Developing barbed microtip-based electrode arrays for biopotential measurement," vol. 14, no. 7, pp. 12370-12386, 2014.

[68] Y. M. Chi, P. Ng, E. Kang, J. Kang, J. Fang, and G. Cauwenberghs, "Wireless non-contact cardiac and neural monitoring," in *Wireless Health 2010*, 2010: ACM, pp. 15-23.

[69] P. Fiedler et al., "Contact pressure and flexibility of multipin dry EEG electrodes," *IEEE Transactions on Neural Systems and Rehabilitation Engineering*, vol. 26, no. 4, pp. 750-757, 2018.

[70] Y.-H. Chen et al., "Soft, comfortable polymer dry electrodes for high quality ECG and EEG recording," *Sensors*, vol. 14, no. 12, pp. 23758-23780, 2014.

[71] X. Tao, *Wearable electronics and photonics*. Elsevier, 2005.

[72] A. Khan, M. Hussain, O. Nur, and M. Willander, "Fabrication of zinc oxide nanoneedles on conductive textile for harvesting piezoelectric potential," *Chemical Physics Letters*, vol. 612, pp. 62-67, 2014.

[73] R. Salvado, C. Loss, R. Gonçalves, and P. Pinho, "Textile materials for the design

of wearable antennas: A survey," *Sensors*, vol. 12, no. 11, pp. 15841-15857, 2012.

[74] E. Hu, A. Kaynak, and Y. Li, "Development of a cooling fabric from conducting polymer coated fibres: Proof of concept," *Synthetic metals*, vol. 150, no. 2, pp. 139-143, 2005.

[75] A. Ostmann, R. Viero, M. Seckel, T. Löher, and H. Reichl, "Stretchable circuit board technology in textile applications," in *2009 4th International Microsystems, Packaging, Assembly and Circuits Technology Conference*, 2009: IEEE, pp. 216-219.

[76] D. Morris, S. Coyle, Y. Wu, K. T. Lau, G. Wallace, and D. Diamond, "Bio-sensing textile based patch with integrated optical detection system for sweat monitoring," *Sensors and Actuators B: Chemical*, vol. 139, no. 1, pp. 231-236, 2009.

[77] J. Kim and G. Cho, "Thermal storage/release, durability, and temperature sensing properties of thermostatic fabrics treated with octadecane-containing microcapsules," *Textile Research Journal*, vol. 72, no. 12, pp. 1093-1098, 2002.

[78] S. D. Min, Y. Yun, and H. Shin, "Simplified structural textile respiration sensor based on capacitive pressure sensing method," *IEEE Sensors Journal*, vol. 14, no. 9, pp. 3245-3251, 2014.

[79] Y.-D. Lee and W.-Y. Chung, "Wireless sensor network based wearable smart shirt for ubiquitous health and activity monitoring," *Sensors and Actuators B: Chemical*, vol. 140, no. 2, pp. 390-395, 2009.

[80] J. Cho, J. Moon, K. Jeong, and G. Cho, "Application of PU-sealing into Cu/Ni electroless plated polyester fabrics for e-textiles," *Fibers and Polymers*, vol. 8, no. 3, pp. 330-334, 2007.

[81] M. Stoppa and A. Chiolerio, "Wearable electronics and smart textiles: a critical review," *sensors*, vol. 14, no. 7, pp. 11957-11992, 2014.

[82] S. H. Lee, S. M. Jung, C. K. Lee, K. S. Jeong, G. Cho, and S. K. Yoo, "Wearable ECG monitoring system using conductive fabrics and active electrodes," in *International Conference on Human-Computer Interaction*, 2009: Springer, pp. 778-783.

[83] G. Cho, K. Jeong, M. J. Paik, Y. Kwun, and M. Sung, "Performance evaluation of

textile-based electrodes and motion sensors for smart clothing," *IEEE Sensors Journal*, vol. 11, no. 12, pp. 3183-3193, 2011.

[84] Y. Zhou, X. Ding, J. Zhang, Y. Duan, J. Hu, and X. Yang, "Fabrication of conductive fabric as textile electrode for ECG monitoring," *Fibers and Polymers*, vol. 15, no. 11, pp. 2260-2264, 2014.

[85] S. Takamatsu, T. Lonjaret, D. Crisp, J.-M. Badier, G. G. Malliaras, and E. Ismailova, "Direct patterning of organic conductors on knitted textiles for long-term electrocardiography," *Scientific reports*, vol. 5, p. 15003, 2015.

[86] K. S. Novoselov and A. Geim, "The rise of graphene," vol. 6, no. 3, pp. 183-191, 2007.

[87] M. K. Yapici, T. Alkhidir, Y. A. Samad, and K. Liao, "Graphene-clad textile electrodes for electrocardiogram monitoring," *Sensors and Actuators B: Chemical*, vol. 221, pp. 1469-1474, 2015.

[88] S. Shang and W. Zeng, "Conductive nanofibres and nanocoatings for smart textiles," in *Multidisciplinary Know-How for Smart-Textiles Developers*: Elsevier, 2013, pp. 92-128.

[89] M. Yapici and T. Alkhidir, "Intelligent medical garments with graphene-functionalized smart-cloth ECG sensors," *Sensors*, vol. 17, no. 4, p. 875, 2017.

[90] X. Tang and X. Yan, "Dip-coating for fibrous materials: mechanism, methods and applications," *Journal of Sol-Gel Science and Technology*, vol. 81, no. 2, pp. 378-404, 2017.

[91] A. Ankhili, X. Tao, C. Cochrane, D. Coulon, and V. Koncar, "Washable and reliable textile electrodes embedded into underwear fabric for electrocardiography (ECG) monitoring," *Materials*, vol. 11, no. 2, p. 256, 2018.

[92] Y. Zhao, Y. Cao, J. Liu, Z. Zhan, X. Li, and W. Li, "Single-Wall Carbon Nanotube-Coated Cotton Yarn for Electrocardiography Transmission," *Micromachines*, vol. 9, no. 3, p. 132, 2018.

[93] A. K. Sen, *Coated textiles: principles and applications*. Crc Press, 2001.

- [94] E. Garcia-Brejjo, G. Prats-Boluda, J. V. Lidon-Roger, Y. Ye-Lin, and J. Garcia-Casado, "A comparative analysis of printing techniques by using an active concentric ring electrode for bioelectrical recording," *Microelectronics International*, vol. 32, no. 2, pp. 103-107, 2015.
- [95] K. S. Novoselov, V. Fal, L. Colombo, P. Gellert, M. Schwab, and K. Kim, "A roadmap for graphene," *nature*, vol. 490, no. 7419, p. 192, 2012.
- [96] J. Molina, "Graphene-based fabrics and their applications: a review," *RSC Advances*, vol. 6, no. 72, pp. 68261-68291, 2016.
- [97] Y.-Z. Wu, J.-X. Sun, L.-F. Li, Y.-S. Ding, and H.-A. Xu, "Performance evaluation of a novel cloth electrode," in *2010 4th International Conference on Bioinformatics and Biomedical Engineering*, 2010: IEEE, pp. 1-5.
- [98] C. L. Lam, N. N. Z. M. Rajdi, and D. H. Wicaksono, "MWCNT/Cotton-based flexible electrode for electrocardiography," in *SENSORS, 2013 IEEE*, 2013: IEEE, pp. 1-4.
- [99] S. Y. Madani, A. Mandel, and A. M. Seifalian, "A concise review of carbon nanotube's toxicology," *Nano reviews*, vol. 4, no. 1, p. 21521, 2013.
- [100] M. Pelin et al., "Differential cytotoxic effects of graphene and graphene oxide on skin keratinocytes," *Scientific reports*, vol. 7, p. 40572, 2017.
- [101] A. Nelson et al., "Wearable multi-sensor gesture recognition for paralysis patients," in *SENSORS, 2013 IEEE*, 2013: IEEE, pp. 1-4.
- [102] G. Paul, R. Torah, S. Beeby, and J. Tudor, "The development of screen printed conductive networks on textiles for biopotential monitoring applications," *Sensors and Actuators A: Physical*, vol. 206, pp. 35-41, 2014.
- [103] X. Guo et al., "A self-wetting paper electrode for ubiquitous bio-potential monitoring," *IEEE Sensors Journal*, vol. 17, no. 9, pp. 2654-2661, 2017.
- [104] C.-T. Lin, L.-D. Liao, Y.-H. Liu, I.-J. Wang, B.-S. Lin, and J.-Y. Chang, "Novel dry polymer foam electrodes for long-term EEG measurement," *IEEE Transactions on Biomedical Engineering*, vol. 58, no. 5, pp. 1200-1207, 2010.

- [105] M. Shateri-Khalilabad and M. Yazdanshenas, "Fabricating electroconductive cotton textiles using graphene," vol. 96, no. 1, pp. 190-195, 2013.
- [106] A. Cömert, M. Honkala, and J. Hyttinen, "Effect of pressure and padding on motion artifact of textile electrodes," vol. 12, no. 1, p. 26, 2013.
- [107] P. Malmivuo, J. Malmivuo, and R. Plonsey, *Bioelectromagnetism: principles and applications of bioelectric and biomagnetic fields*. Oxford University Press, USA, 1995.
- [108] J. Keegan, E. Burke, and J. Condrón, "An electrooculogram-based binary saccade sequence classification (BSSC) technique for augmentative communication and control," in *2009 Annual International Conference of the IEEE Engineering in Medicine and Biology Society*, 2009: IEEE, pp. 2604-2607.
- [109] K. Pettersson, S. Jagadeesan, K. Lukander, A. Henelius, E. Hægström, and K. Müller, "Algorithm for automatic analysis of electro-oculographic data," *Biomedical engineering online*, vol. 12, no. 1, p. 110, 2013.
- [110] J. Heo, H. Yoon, and K. Park, "A novel wearable forehead EOG measurement system for human computer interfaces," vol. 17, no. 7, p. 1485, 2017.
- [111] H. Manabe and M. Fukumoto, "Full-time wearable headphone-type gaze detector," in *CHI'06 Extended Abstracts on Human Factors in Computing Systems*, 2006: ACM, pp. 1073-1078.
- [112] Y.-F. Zhang, X.-Y. Gao, J.-Y. Zhu, W.-L. Zheng, and B.-L. Lu, "A novel approach to driving fatigue detection using forehead EOG," in *2015 7th International IEEE/EMBS Conference on Neural Engineering (NER)*, 2015: IEEE, pp. 707-710.
- [113] E. S. Valchinov and N. E. Pallikarakis, "An active electrode for biopotential recording from small localized bio-sources," *BioMedical Engineering OnLine*, vol. 3, no. 1, p. 25, 2004.
- [114] T.-H. Kang, C. R. Merritt, E. Grant, B. Pourdeyhimi, and H. T. Nagle, "Nonwoven fabric active electrodes for biopotential measurement during normal daily activity," *IEEE Transactions on Biomedical Engineering*, vol. 55, no. 1, pp. 188-195, 2007.
- [115] T. Yagi, Y. Kuno, K. Koga, and T. Mukai, "Drifting and blinking compensation in

electro-oculography (EOG) eye-gaze interface," in 2006 IEEE International Conference on Systems, Man and Cybernetics, 2006, vol. 4: IEEE, pp. 3222-3226.

[116] E. Alexandridis, E. Ariely, and G. O. Gronau, "Einfluß der Bulbuslage und der Bulbuslänge auf das EOG," vol. 194, no. 4, pp. 237-241, 1975.

[117] M. M. Puurtinen, S. M. Komulainen, P. K. Kauppinen, J. A. Malmivuo, and J. A. Hyttinen, "Measurement of noise and impedance of dry and wet textile electrodes, and textile electrodes with hydrogel," in 2006 International Conference of the IEEE Engineering in Medicine and Biology Society, 2006: IEEE, pp. 6012-6015.

[118] A. A. Chlahawi, B. B. Narakathu, S. Emamian, B. J. Bazuin, M. Atashbar, "Development of printed and flexible dry ECG electrodes," vol. 20, pp. 9-15, 2018.

[119] X. An and G. J. M. Stylios, "A Hybrid Textile Electrode for Electrocardiogram (ECG) Measurement and Motion Tracking," vol. 11, no. 10, p. 1887, 2018.

[120] J. Otero-Millan, S. L. Macknik, and S. Martinez-Conde, "Fixational eye movements and binocular vision," vol. 8, p. 52, 2014.

[121] K. Kaneko and K. Sakamoto, "Evaluation of three types of blinks with the use of electro-oculogram and electromyogram," vol. 88, no. 3, pp. 1037-1052, 1999.

[122] T. Nakano, Y. Yamamoto, K. Kitajo, T. Takahashi, and S. Kitazawa, "Synchronization of spontaneous eyeblinks while viewing video stories," vol. 276, no. 1673, pp. 3635-3644, 2009.

## **Appendix A**

The experimental procedures involving volunteer human subjects described in this research are followed by the ethical principles outlined in the Helsinki Declaration of 1964, as revised in 2013 and participants gave their informed consent for inclusion before they participated in the study. The authors gratefully thank the participants involved in this study.



## Appendix B: Supplementary Information

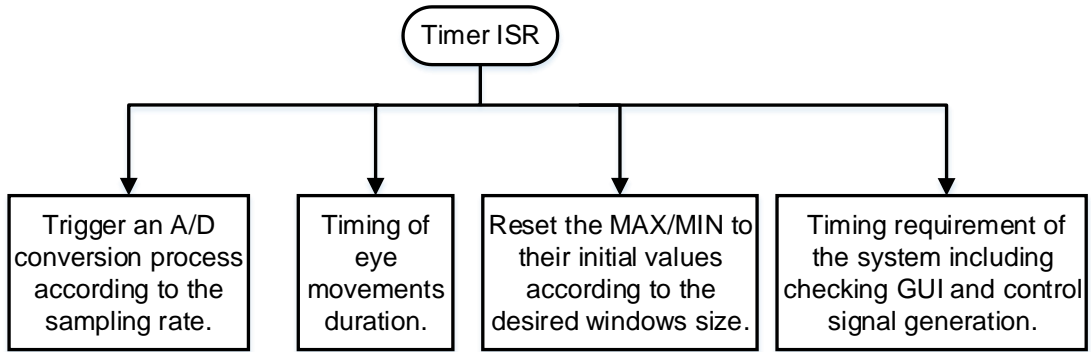


Figure S1. Timer Interrupt Serves Routine working block diagram for proposed embedded software.

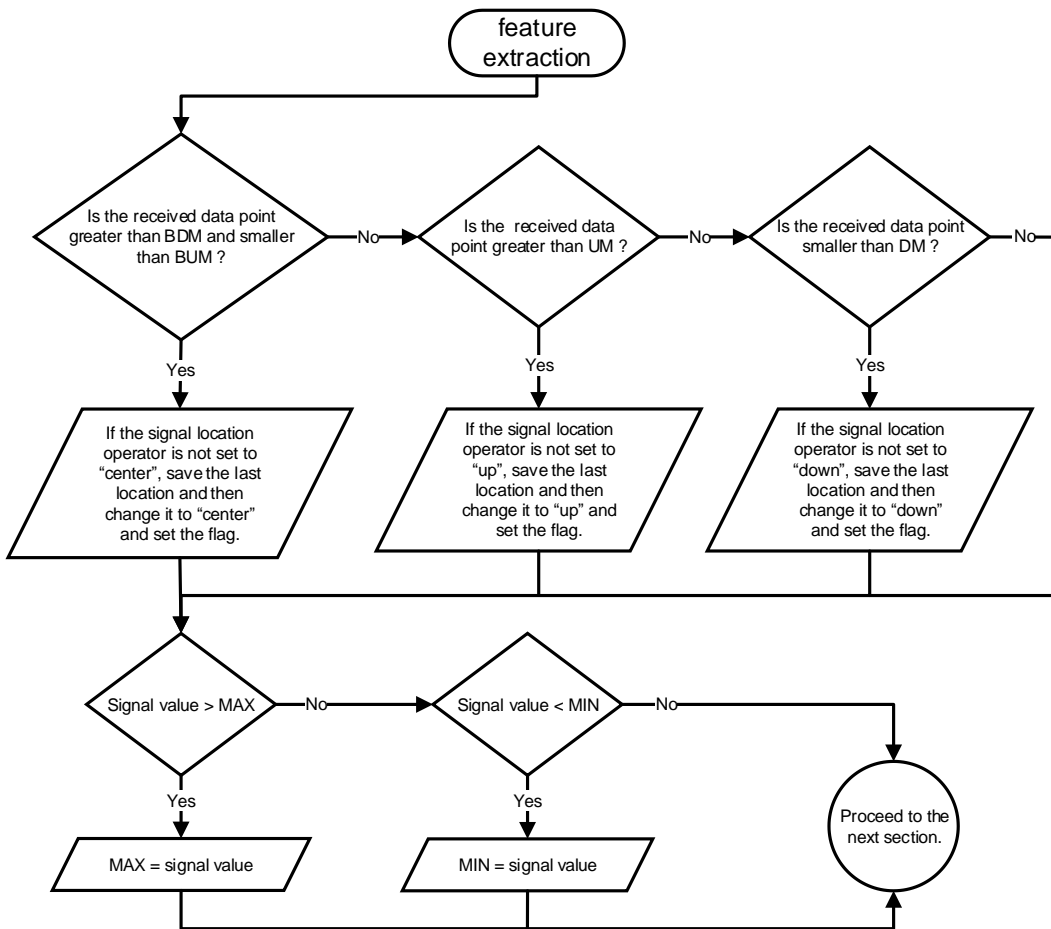


Figure S2. The detailed feature extraction section of the flowchart for the proposed automatic EM detection algorithm.

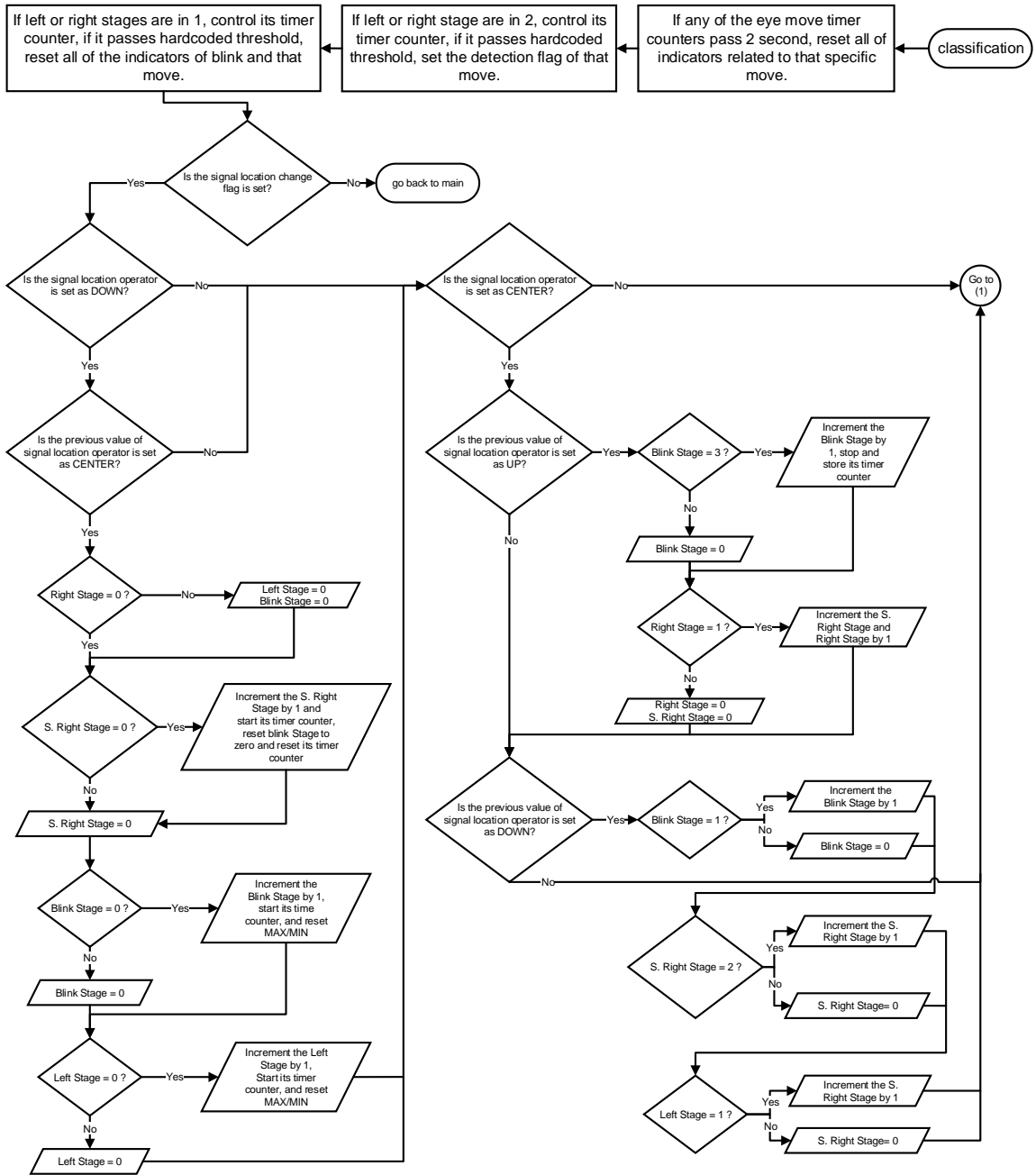


Figure S3. The first part of the detailed classification section of the flowchart for the proposed automatic EM detection algorithm. (S: Swift)

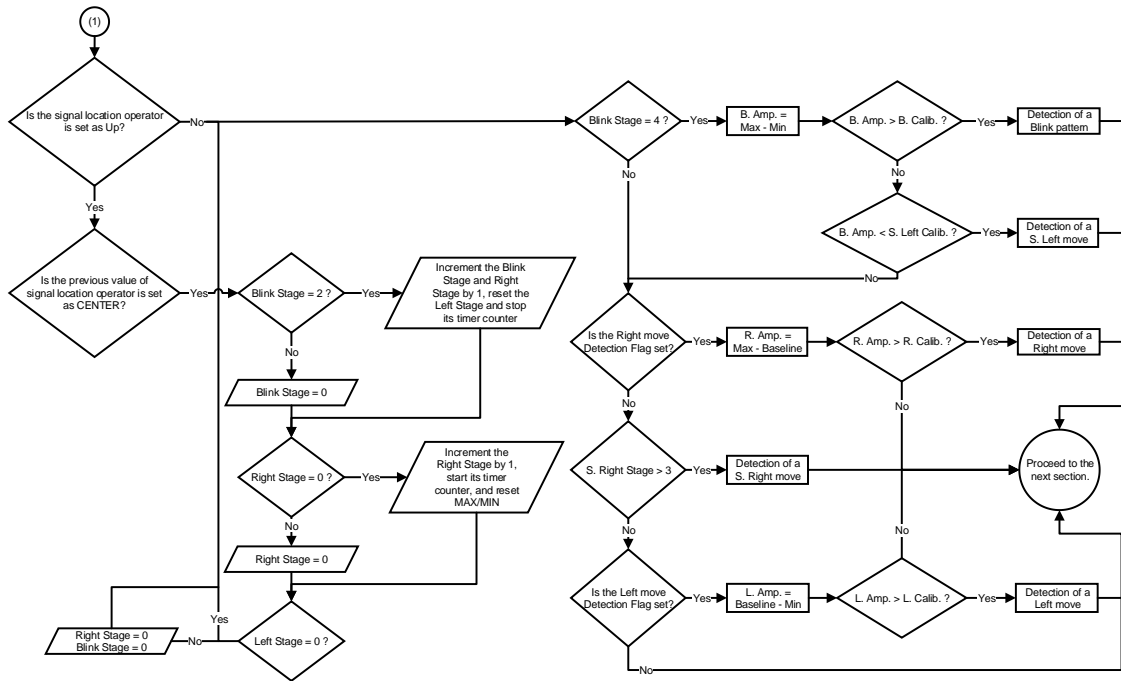


Figure S4. The second part of the detailed classification section of the flowchart for the proposed automatic EM detection algorithm. (S: swift, B: volunteer blink, L: left movement, R: right movement, Amp: amplitude, Calib: calibration)